Antenna Beamforming for Infrastructureless Wireless Networks

by

Elizabeth C. Godoy

Submitted to the Department of Electrical Engineering and Computer Science

in Partial Fulfillment of the Requirements for the Degree of

Master of Engineering in Electrical Engineering and Computer Science

at the

MASSACHUSETTS INSTITUTE OF TECHNOLOGY

May 2007

[June 2007]

Author_____

Department of Electrical Engineering and Computer Science

May 31, 2007

Certified by_____

Vincent W. S. Chan

Joan and Irwin M. Jacob Professor of EECS and Aero/Astro

Director, Laboratory for Information and Decision Systems

Thesis Supervisor

Accepted by_____

Arthur C. Smith

Professor of Electrical Engineering

Chairman, Department Committee on Graduate Theses

Antenna Beamforming for Infrastructureless Wireless Networks

by

Elizabeth C. Godoy

Submitted to the Department of Electrical Engineering and Computer Science
on May 31, 2007, in partial fulfillment of
the requirements for the degree of
Master of Engineering in Electrical Engineering and Computer Science

Abstract

Our work studies the impact of antenna beamforming on the performance of infrastructureless wireless networks. Based on examination of the beampattern for a uniform circular antenna array (UCAA) utilizing beamforming under a constraint on maximum average transmit power, we approximate achievable user data rates as a function of the number of antenna elements, and we examine the behavior of these rates in a simple network with varying noise power and interference and with different scheduling of user transmissions. We find that user data rates increase with the number of antenna elements up to a point of saturation determined by the antenna size and carrier wavelength. Moreover, in some cases that we outline, judicious scheduling of user transmissions can increase achievable data rates.

Thesis Supervisor: Vincent W. S. Chan
Title: Joan and Jacob Professor of EECS and Aero/Astro
Director, Laboratory for Information and Decision Systems

Acknowledgements

I would like to thank Lillian Dai and Professor Chan for their unwavering support and guidance, without which this work would not have been possible. Lillian's help at every step in the process of creating this thesis proved invaluable. In addition, I am fortunate to have had Professor Chan as an advisor and am grateful to him for providing me with the opportunity to do this work and also for offering his insights and wisdom. I am also grateful to DARPA for providing the financial support for this research. Thank you, as well, to my officemates and the administrative staff, who have made my time at LIDS enjoyable.

Most importantly, thank you to my parents for providing me with the foundation to learn and grow. To my parents, brother and family: you are the source of my strength.

Finally, thank you to my friends for making my world at MIT entertaining and memorable. Your support and friendship have kept me sane and smiling.

Table of Contents

List of Figures

List of Tables

Chapter 1

Introduction

Technological advances in wireless communications over the past few decades have revolutionized the way by which people interact. From cell phones to any of the assortment of devices used for wireless Internet access, it has never been easier to remain connected to the global telecommunication network. One technological advance that has received much attention in the wireless communications field is multiple antenna element systems. Such systems find applications for both optical and radio frequency (RF) antennas in satellite, cellular, and ad-hoc wireless communications. In contrast to wireless devices that use a single omnidirectional or directional antenna, wireless devices that use multiple transmit and/or receive antenna elements can better combat channel fading through diversity, and attain higher data throughput by concentrating power in desired directions and suppressing interference in undesired directions.

One particular way of utilizing multiple antenna elements in wireless networks is antenna beamforming. By controlling the phase and amplitude of the signal field at each antenna element, the radiated electromagnetic (EM) field can be patterned to have high antenna gains in desired directions and low antenna gains in undesired directions. Such a multiple antenna element system is termed a beamforming antenna array.

Antenna beamforming has found a diverse range of applications, including satellite [1] and cellular [2]-[4] wireless communications. In recent years, many proposed using antenna arrays in ad-hoc wireless networks [5]-[16]. Since many ad-hoc wireless networks are interference-limited [17], antenna arrays can significantly increase network

data rates over systems with omnidirectional antennas. However, practical implementations of antenna arrays for such networks are few and far in between. For cellular networks, directional and sectoral antennas are typically used. For mobile wireless networks, one of the main challenges is the lack of location tracking in conventional ad-hoc wireless networks, making it difficult to adapt the antenna radiation pattern to the changing user locations. Proactive Mobile Wireless Networks, as presented in [18], offers an example of a type of infrastructureless wireless network in which the positions of wireless users are available from localization and trajectory prediction. With these additional capabilities, antenna arrays can be more effectively used in a mobile wireless network environment.

The primary goal of this thesis is to study the impact of antenna beamforming on the performance of infrastructureless wireless networks. We present analytical expressions for the radiated field of an antenna array as a function of the array size and number of antenna elements. With these expressions, the antenna directivity; interference, and achievable data rates in a multi-user environment can be found. In addition to beamforming, we also examine the effects and address the potential benefits of scheduling transmissions in the network to further reduce interference. Since the joint antenna beamforming, power allocation, and scheduling problem does not lend itself to analytical studies, instead of resorting to numerical and algorithmic studies, we attempt to gain some insights on the achievable data rates by studying a simple network with three users located at the vertices of an equilateral triangle.

Our contributions include:

- A model approximating directivity and interference levels generated by a single antenna array.
- A study of the impact of interference on achievable data rates in a simple three-user network.
- Insights into how beamforming, power allocation, and scheduling affect user data rates in infrastructureless wireless networks.

This dissertation is organized as follows. We present the problem setup in chapter 3 and outline the models and assumptions that we use throughout our work. Chapter 4 reviews the physics of radiating antennas while Chapter 5 examines beamforming for aperture and array antennas in an infrastructureless wireless network context. Chapter 6 makes approximations to the beam sidelobe levels based on the density of array elements and then uses these approximations to analyze interference in the network. Chapter 7 summarizes the beamforming, power and interference analyses in the previous chapters and examines the achievable data rates in a simple network. The last section of Chapter 7 examines achievable data rates and compares the network performance for different power allocation and scheduling schemes. Finally, Chapter 8 concludes our work and proposes future research directions based on our findings.

Chapter 2

Background

This thesis is primarily motivated by [1] on joint antenna array beamforming and scheduling for satellite communications. The work in [1] examines beamforming for satellite transmissions from an *antenna aperture* to multiple users on Earth. An antenna aperture, in the context of [1] and as used in this thesis, is an antenna of finite size with an infinite number of infinitesimal antenna elements. In addition to beamforming, [1] also considers the benefits of scheduling in scenarios where users experience a high level of interference. In this thesis, we seek to extend the analysis presented in [1] to an infrastructureless wireless network scenario within the architectural framework of Proactive Mobile Wireless Networks.

The antenna model used in [1] cannot be directly carried over to our problem for two reasons. First, for satellite communications, the antenna on the satellite in space is transmitting to users on the Earth, approximately normal to the antenna, as shown in Fig. 2.1. In [1], the antenna aperture radiation field is taken directly from the results of scalar diffraction theory with the Fraunhofer approximation. In scalar diffraction theory, the field at the aperture is adequately modeled by "secondary radiating sources," each radiating EM fields that are maximized in the direction normal to the aperture and diminished in the directions away from the normal [19]. For the scenario in [1], the directivity of these secondary radiating sources in the direction of the users is approximately constant since the users are all located around a region close to the normal direction. For infrastructureless wireless network communications, users transmit to and

receive from other users on the same plane, as shown in Fig. 2.2. For simplicity, in this thesis, we examine beamforming for circular arrays oriented parallel to the ground so there is rotational symmetry in the radiated beam pattern in any direction.

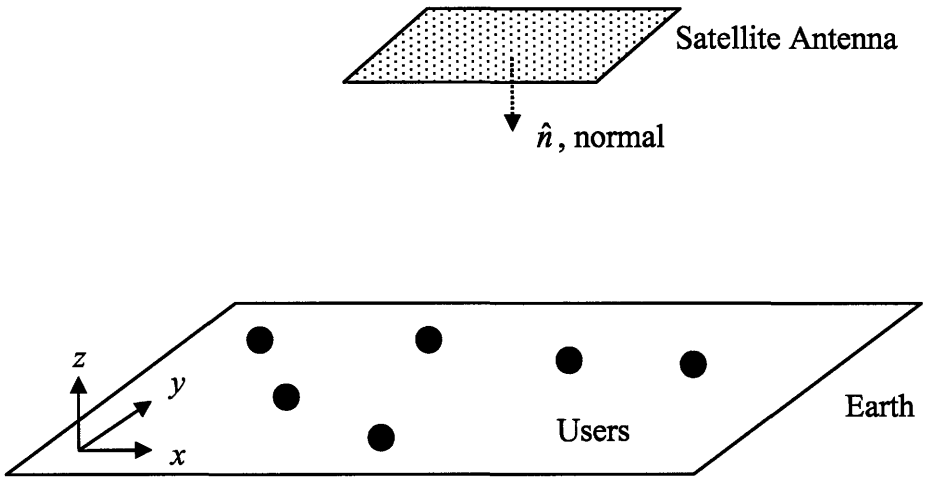

Fig. 2.1. A satellite rectangular aperture antenna serving users on the Earth.
(x,y and z are the axes labels in the Cartesian coordinate system, $\hat{n}$ is the normal vector to the antenna)

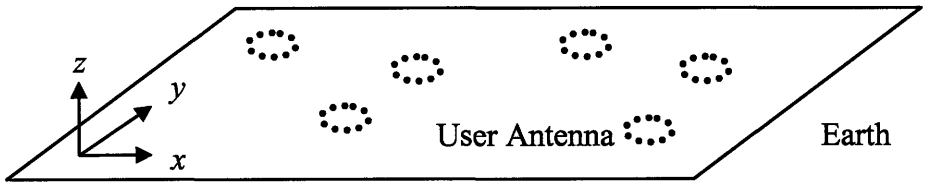

Fig 2.2. An infrastructureless wireless network of users with antenna arrays on the ground.

Second, [1] considers beamforming for a continuous antenna aperture in which the phase and amplitude of the antenna field can be adjusted at all points on a continuous surface. Our work, on the other hand, addresses beamforming for a discrete array of antenna elements, with a continuous aperture as a limiting case. As we will discuss in Chapter 3, our study will focus only on the radiation pattern due to array geometry. In doing so, each point on the array is appropriately modeled as an isotropic radiating source as opposed to a secondary source with directivity. In extending the beamforming analysis in [1] to infrastructureless networks, the directive gains of a discrete array antenna approach that of a continuous aperture of the same size.

Like [1], we consider an idealized channel model without fading or scattering in the environment in order to understand the basic properties and effects of beamforming on achievable user data rates. We also consider beamforming with scheduling among the users to explore the potential benefits of scheduling user transmissions in scenarios with different noise and interference levels.

Chapter 3

Problem Set-Up

This thesis seeks to study the impact of antenna arrays on infrastructureless wireless network performance, albeit in an idealized setting. The network model under consideration will be described in this chapter. This includes a discussion of the wireless scenario and several simplifying assumptions. We will also describe the antenna model including the particular antenna geometry and beamforming scheme that we consider.

3.1 Network Model

We consider a network of M users, indexed by $j = 1,...M$, each operating in a planar surface as shown in Fig. 2.2. These users may be mobile and are assumed to have means to determine their relative locations at any time. The users (or nodes) are wirelessly enabled and automatically discover other nodes within their communication range. In addition, each user is equipped with a multiple antenna element array and utilizes beamforming to transmit to and receive from any of the other M-1 users. Details of the antenna model will be provided in the next section. Typically, these un-tethered nodes operate on batteries; therefore, the maximum amount of power that each user can transmit on average is limited. Let the maximum average power be denoted by P_{tot}. Consequently, the total time-averaged radiated power P_{rad} for each transmitting antenna must be less than or equal to P_{tot}, i.e. $P_{rad} \leq P_{tot}$.

We assume that the RF power decreases with distance according to a free-space propagation model. In a real world environment, there are often RF absorbers and/or scatterers between a transmitter and receiver. For simplicity, we suppress these effects in our work and focus rather on the most basic, idealized channel model. Given the network model described above, we can now consider performance for simple infrastructureless wireless networks.

Individual achievable data rate is an important performance metric for wireless networks. Since we assume a obstacle-free channel, the wireless link can be modeled as an additive white Gaussian noise (AWGN) channel. With appropriate signal coding, we assume that rates near the Shannon Capacity can be achieved. This yields user data rate R_{ij} for transmissions from user i to user j,

$$R_{ij}[bits/\sec] = W\log_2(1+\mathrm{SINR}_{ij}) \tag{3.1}$$

where W is the channel bandwidth and the signal-to-interference-and-noise ratio, SINR_{ij}, is the received signal power from i divided by the sum of interference powers from other transmitters and thermal noise power.

3.2 Antenna Model

An antenna is a device through which electromagnetic (EM) waves are transmitted and received. Each user's antenna can consist of a single omni-directional antenna, a directional antenna aperture, or multiple antenna elements. In this work, we consider antennas with multiple antenna elements that can concentrate power in any

direction and adaptively change the direction based on user locations. The ability and means by which these antennas can focus power depends on the spatial distribution, orientation of the antenna elements, and user locations.

The particular antenna geometry that we consider in our work is a uniform circular antenna array (UCAA) oriented on the x-y plane as shown in Fig. 2.2. On this plane, a circular array is the simplest geometry for achieving radiation symmetry in all directions. Each UCAA consists of N antenna elements, indexed by $n = 0,...N-1$, equally spaced along the circumference of a circle of radius R, as shown in Fig. 3.1.

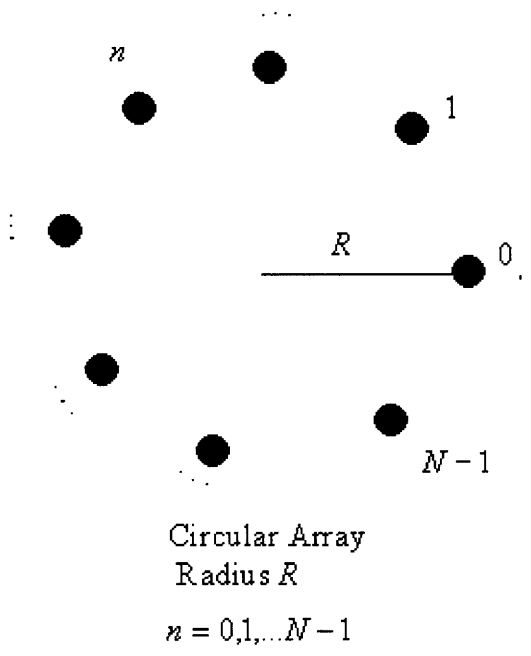

Fig. 3.1 Uniform Circular Antenna Array (UCAA).

The signals arriving at or radiating from the antenna elements will be delayed depending on the antenna geometry and orientation of the elements relative to the direction of observation. The goal of beamforming is to adjust for these delays so that

power gain in the desired directions is maximized. In the farfield (or Fraunhofer region) where the receiving antenna is at least a distance $\frac{2L^2}{\lambda}$ from the transmitting antenna (L is the maximum linear dimension of the antenna, and λ is the carrier wavelength), any radiated field will appear as a plane wave to the receiving antenna [19, 20]. This assumption decouples beamforming on transmit and receive, allowing us to determine the appropriate beamforming scheme at one end of the wireless link independently of that at the other.

There are several beamforming schemes for achieving a desired beam pattern as outlined in [21]. In this thesis, we consider a baseline method called *conventional beamforming* that compensates for the spatial delays of the antenna elements such that the radiated or received signals from desired directions add coherently. For narrowband transmissions in which the signal bandwidth is typically less than 5% of the carrier frequency, the spatial delays can be well approximated by phase shifts. In addition to phase shifts, the signal amplitude at each antenna element can be adjusted. For conventional beamforming, the signal amplitude adjustment is set to be uniform across the antenna elements. The constant amplitude and relative phase adjustments constitute complex weights that can be varied at each antenna element to change the antenna beam pattern.

The radiation pattern of an antenna with elements that are identical can be expressed as the product of a single element's radiation pattern and a linear superposition of the fields radiated from each of the element sources, modeled as isotropic and infinitesimally small. This superposition sum or integral, called the *array factor*, captures the interference pattern among the fields radiated from the antenna elements,

incorporating the geometry of the antenna and the relative spacing of the elements. The array factor is independent of the particular type of element utilized at the array, which is physically modeled by a radiation pattern for a single element. Factoring out this single element radiation pattern from the linear array factor is called *array factorization*. In this work, we consider the antenna elements as isotropically radiating point sources and note that an actual physical implementation of an antenna can be incorporated into our development by scaling the array factor by an individual element radiation pattern.

For an antenna with a fixed size, we can theoretically pack the antenna with an arbitrarily large number of infinitesimally small isotropic antenna elements. In practice, when antenna element spacing is closer than $\frac{\lambda}{2}$, significant mutual coupling among antenna elements occur and distorts the radiation pattern [22]. In this thesis, we assume no mutual coupling among the antenna elements as a first-order study, keeping in mind that the results presented in this thesis do not hold for densely packed arrays with antenna element spacing much closer than $\frac{\lambda}{2}$. With the no mutual coupling assumption, the number of antenna elements in an antenna with fixed size can approach infinity, which models a continuous aperture. In our setup with a UCAA, as the number of antenna elements approaches infinity, the antenna array will approach a continuous ring aperture, as shown in Fig. 3.2. Conversely, we can consider antenna arrays with discrete antenna elements as spatial samplings of a continuous aperture, where each sampled point is an isotropic antenna element.

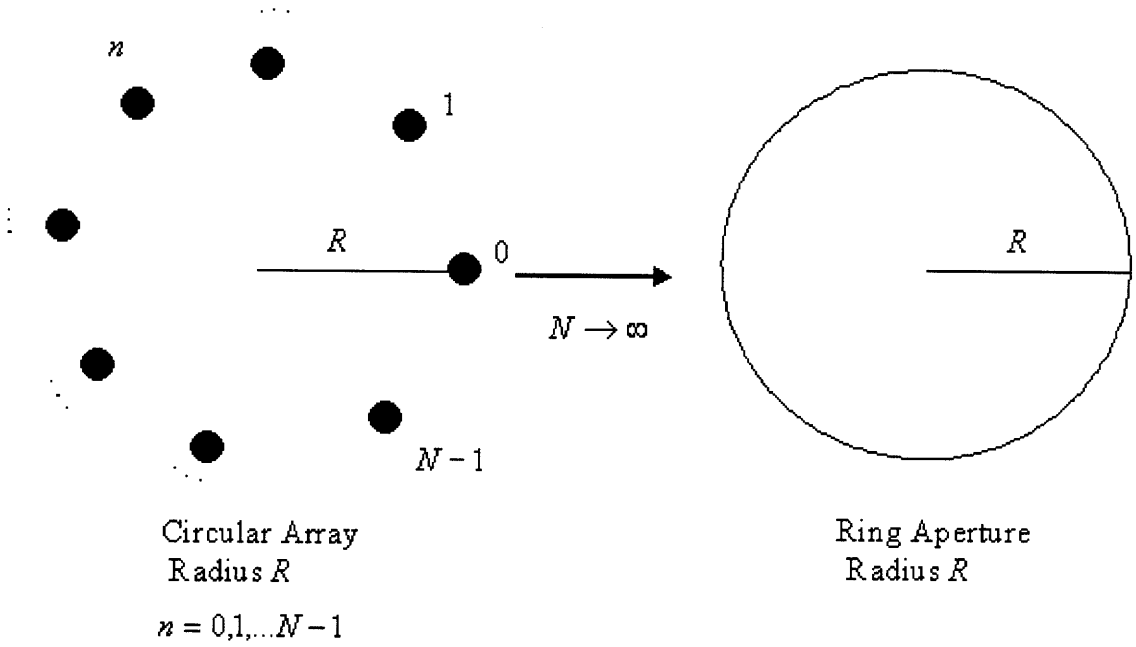

Fig. 3.2 Uniform circular antenna array (UCAA) and continuous ring aperture.

Chapter 4

Antenna Radiation Field Review

This chapter presents a background of the physics behind a radiating aperture with our antenna model described in Chapter 3. Working from electromagnetic (EM) wave theory and applying our assumptions on the antenna model, we find analytical expressions for the transmit EM field, total radiated power, and antenna directivity.

4.1 Aperture Radiation Field

In order to gain some insights into how antenna beamforming affect wireless user data rates, we consider the field pattern influenced by array geometry and not by individual antenna element radiation patterns. As described in Chapter 3, the influence of the antenna geometry is captured completely by the array factor. The array factor describes the antenna radiation field under the assumption that antenna elements are infinitesimal isotropic sources. Note that this model for antenna elements is an idealization in that these sources do not exist in reality. However, we can use this model for antenna elements without loss of insight and, due to array factorization, also without loss of generality.

In addition to our assumption that the antenna elements are isotropic sources, recall from Chapter 3 that we also assume that these antenna elements do not interact with each other in any way (ie. no mutual coupling). With this antenna model, we can begin with the EM field radiated from a single antenna element and then linearly

superimpose the fields radiated from each of these point sources to find the total radiated field of an antenna. Fig. 4.1 shows an antenna element location indicated by the vector $\bar{r}'$ and an observation location $\bar{r}_0$ in the Fraunhofer farfield region, with $\hat{r}_0$ representing the unit vector along this direction. The distance between the source and point of observation is $\left|\bar{r}_0 - \bar{r}'\right|$. The radiation field $U(\bar{r}_0)$ (either E or H field) due to this single isotropic source is given in (4.1), where $k = \frac{2\pi}{\lambda}$ (commonly called wavenumber) and V is a proportionality constant [22]. For simplicity and clarity of exposition, we will suppress this constant throughout the remainder of this thesis.

$$U(\bar{r}_0) = V\frac{1}{j\lambda}\frac{\exp\left(jk\left|\bar{r}_0 - \bar{r}'\right|\right)}{\left|\bar{r}_0 - \bar{r}'\right|} \tag{4.1}$$

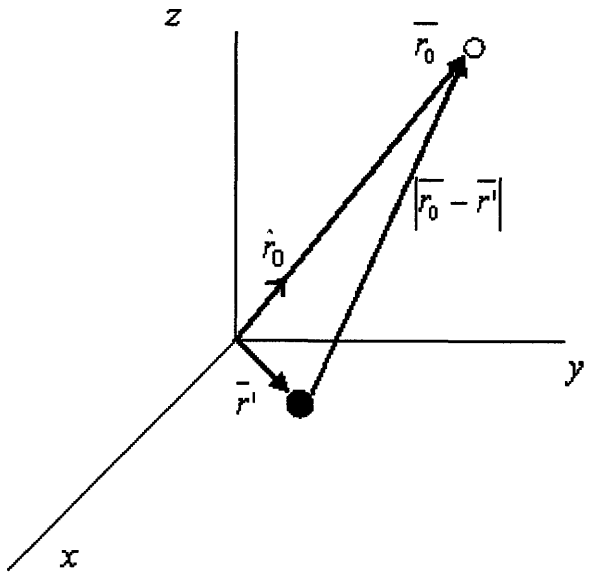

Fig. 4.1. Diagram of a single antenna element located at $\bar{r}'$ and a point of observation in the farfield at $\bar{r}_0$.

Superimposing the fields due to each of the elements along an aperture surface *S*, we find the total radiated field at a point of observation $\bar{r}_0$ in the farfield of the aperture antenna given by (4.2).

$$U(\bar{r}_0) = \frac{1}{j\lambda} \iint_S \frac{\exp\left(jk|\bar{r}_0 - \bar{r}'|\right)}{|\bar{r}_0 - \bar{r}'|} ds \tag{4.2}$$

With the farfield radiation approximation, $|\bar{r}_0 - \bar{r}| \approx r_0 - \hat{r}_0 \cdot \bar{r}$, $(kr_0 >> 1)$, and assuming that the distance from each point on the aperture to the point of observation is approximately equal outside of the exponent, $\frac{1}{r_0 - \hat{r}_0 \cdot r} \cong \frac{1}{r_0}$, this field expression simplifies to (4.3) [20].

$$U(\overline{r_0}) = \frac{1}{j\lambda}\frac{\exp(jkr_0)}{r_0}\iint_S \exp(-jk\hat{r}_0 \cdot \overline{r'})ds \tag{4.3}$$

Since the antenna aperture we consider is a ring, it is more natural to express the field expression in spherical coordinates. We use standard spherical coordinate notation as shown in Fig. 4.2. For a ring aperture with radius R on the x-y plane with $\theta' = \frac{\pi}{2}$, the radiated field expressed in spherical coordinates is given by (4.4), where we have used the equality $\hat{r}_0 \cdot \overline{r'} = R\sin\theta_0 \cos(\phi' - \phi_0)$.

$$U(d_0, \theta_0, \phi_0) = \frac{1}{j\lambda}\frac{\exp(jkd_0)}{d_0}\int_0^{2\pi} \exp\big(-jkR\sin\theta_0 \cos(\phi' - \phi_0)\big)Rd\phi' \tag{4.4}$$

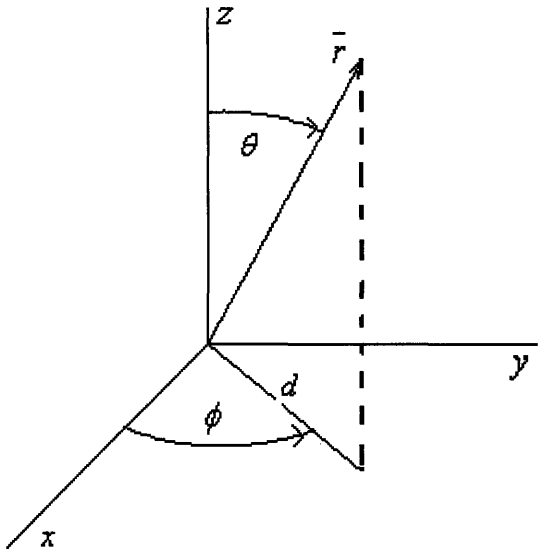

$$d = \sqrt{x^2 + y^2}$$

$$\bar{r} = r \begin{bmatrix} \sin\theta\cos\phi \\ \sin\theta\sin\phi \\ \cos\theta \end{bmatrix}$$

Fig. 4.2. Coordinate System.

4.2 Radiated Power and Directive Gain

In Chapter 3, we discussed the impact of radiated power on the user data rate. From the field equation in (4.4), the total time-averaged radiated power from an individual transmitting aperture can be shown to be (4.5) [20]. Moreover, the radiated power in the desired direction and in the direction of interfering users will determine the signal gain and interference levels in the network. The directive gain, or simply gain, $G(\theta,\phi)$ is defined as the ratio of power along the specified radial (θ,ϕ) to the total

radiated power over 4π steradians (4.6) [20]. The maximum directive gain is called *directivity*, denoted by D (4.7). We will make extensive use of these expressions in our beamforming analysis in subsequent chapters.

$$P_{rad} = \int_0^{2\pi}\int_0^{2\pi} |U(d,\theta,\phi)|^2 d^2 \sin\theta d\phi d\theta \tag{4.5}$$

$$G(\theta,\phi) = \frac{|U(d,\theta,\phi)|^2}{P_{rad}/4\pi d^2} = \frac{4\pi|U(d,\theta,\phi)|^2}{\int_0^{2\pi}\int_0^{2\pi} |U(d,\theta,\phi)|^2 \sin\theta d\phi d\theta} \tag{4.6}$$

$$Directivity = D = G(\theta,\phi)_{\max} \tag{4.7}$$

Chapter 5

Aperture and Array Beamforming

In this chapter, we present expressions describing the fields radiated by antenna apertures and arrays with beamforming. First, we consider the scenario where a single transmitter, utilizing conventional beamforming, transmits to a single receiver with a constraint of maximum average radiated power. We then note the symmetry in receive antenna beamforming and describe the maximum signal gain on an individual wireless link with conventional beamforming utilized on both the transmitting and receiving ends. Next, we extend the beamforming analysis to the case where a single multiple element antenna transmits different information, possibly at different power levels, to spatially distributed users. Finally, we outline the corresponding power allocation problem for the case where multiple users transmit and receive simultaneously in an infrastructureless wireless network.

5.1 Continuous Aperture Beamforming

We first focus on antenna beamforming for a ring aperture of radius R, centered at the origin of the x-y plane, transmitting a signal to a user located at (d_0, θ_0, ϕ_0). The signal radiated from each point on the antenna is multiplied by a complex weight that varies with ϕ' along the ring aperture. The complex weight at the antenna, $w(\phi')$, can be written as:

$$w(\phi') = a_c \exp\left(j\psi(\phi')\right) \tag{5.1}$$

where a_c is a constant with the subscript 'c' denoting a continuous aperture, and $\psi(\phi')$ is a complex phase term that is a function of ϕ'. With this complex weighting, the radiated aperture field at (d_0, θ_0, ϕ_0) becomes:

$$\begin{aligned} U(d_0,\theta_0,\phi_0) &= \frac{1}{j\lambda}\frac{\exp(jkd_0)}{d_0}\int_0^{2\pi} w(\phi')\exp\left(-jkR\sin\theta_0\cos(\phi'-\phi_0)\right)Rd\phi' \\ &= \frac{a_c R}{j\lambda}\frac{\exp(jkd_0)}{d_0}\int_0^{2\pi}\exp\left(j\psi(\phi')\right)\exp\left(-jkR\sin\theta_0\cos(\phi'-\phi_0)\right)d\phi' \end{aligned} \tag{5.2}$$

The phase function, $\psi(\phi')$, ensuring that the product of exponentials in (5.2) is equal to one for all ϕ' and, therefore, maximizing the radiated field at (d_0, θ_0, ϕ_0), is

$$\psi(\phi') = kR\sin\theta_0\cos(\phi'-\phi_0) \tag{5.3}$$

This function serves to counter the effects of spatial delays to ensure that the fields radiating from all points on the aperture arrive at the desired location in phase. With this phase, we have the conventional beamforming weights for a ring aperture and radiated field at any point of observation in the farfield, (d, θ, ϕ), given by (5.4) and (5.5), respectively.

$$w(\phi') = a_c \exp\left(jkR\sin\theta_0\cos(\phi'-\phi_0)\right) \tag{5.4}$$

$$U(d,\theta,\phi) = \frac{a_c R}{j\lambda}\frac{\exp(jkd)}{d}\int_0^{2\pi}\exp\left(jkR\sin\theta_0\cos(\phi'-\phi_0)\right)\exp\left(-jkR\sin\theta\cos(\phi'-\phi)\right)d\phi' \tag{5.5}$$

The amplitude a_c is limited by the maximum average power constraint. Assuming the signal to be transmitted has unit amplitude, the total time-averaged radiated power of the antenna, from (4.5), is

$$\begin{aligned} P_{rad} &= a_c^2\frac{R^2}{\lambda^2}\int_0^{2\pi}\int_0^{2\pi}\left|\int_0^{2\pi}\exp\left(jkR\sin\theta_0\cos(\phi'-\phi_0)\right)\exp\left(-jkR\sin\theta\cos(\phi'-\phi)\right)d\phi'\right|^2\sin\theta d\phi d\theta \\ &= a_c^2\frac{R^2}{\lambda^2}\int_0^{2\pi}\int_0^{2\pi}\left|F_c(\theta,\phi)\right|^2\sin\theta d\phi d\theta \end{aligned} \tag{5.6}$$

where $F_c(\theta,\phi)$ is the array factor for a continuous aperture (5.7).

$$F_c(\theta,\phi) = \int_0^{2\pi}\exp\left(jkR\sin\theta_0\cos(\phi'-\phi_0)\right)\exp\left(-jkR\sin\theta\cos(\phi'-\phi)\right)d\phi' \tag{5.7}$$

Given the average power constraint $P_{rad} \le P_{tot}$, a_c is upper bounded as

$$a_c^2 \le \frac{P_{tot}\lambda^2}{R^2\int_0^{2\pi}\int_0^{2\pi}\left|F_c(\theta,\phi)\right|^2\sin\theta d\phi d\theta} \tag{5.8}$$

With the complex weights described in (5.4) and the corresponding continuous array factor in (5.7), the achievable directivity (4.7) utilizing conventional beamforming on an aperture is

$$
\begin{aligned}
D_{Aperture} &= \frac{4\pi\left|U(d_0,\theta_0,\phi_0)\right|^2}{\int_0^{2\pi}\int_0^{2\pi}\left|U(d,\theta,\phi)\right|^2 \sin\theta d\phi d\theta} \\
&= \frac{4\pi\left|F_c(\theta_0,\phi_0)\right|^2}{\int_0^{2\pi}\int_0^{2\pi}\left|F_c(\theta,\phi)\right|^2 \sin\theta d\phi d\theta} \\
&= \frac{4\pi(2\pi)^2}{\int_0^{2\pi}\int_0^{2\pi}\left|F_c(\theta,\phi)\right|^2 \sin\theta d\phi d\theta}
\end{aligned}
\tag{5.9}
$$

As is evident in (5.9), the directivity does not have a simple closed form expression. We will later use Matlab to numerically calculate this directivity and then compare the results to that of an *N*-element array. We will now present the radiated field of a discrete antenna array with conventional beamforming, under the same transmit power constraint.

5.2 Multiple Element Array Beamforming

With the model of antenna elements as infinitesimal isotropically radiating point sources, an array is simply an aperture sampled with spatial impulses. The total field at a point of observation in the farfield is then a sum of the field from each of the discrete

antenna array elements. For an N-element UCAA with elements spaced uniformly along a ring of radius R, the transmit antenna array field at (d_0, θ_0, ϕ_0) under conventional beamforming is

$$\begin{aligned} U(d_0,\theta_0,\phi_0) &= \frac{1}{j\lambda}\frac{\exp(jkd_0)}{d_0}\sum_{n=0}^{N-1} w(\phi'_n)\exp\left(-jkR\sin\theta_0\cos(\phi'_n-\phi_0)\right) \\ &= \frac{a_d}{j\lambda}\frac{\exp(jkd_0)}{d_0}\sum_{n=0}^{N-1}\exp\left(jk\psi(\phi'_n)\right)\exp\left(-jkR\sin\theta_0\cos(\phi'_n-\phi_0)\right) \end{aligned} \tag{5.10}$$

$$\text{where } w(\phi'_n) = a_d\exp\left(j\psi(\phi'_n)\right) \tag{5.11}$$

and $\phi'_n = \frac{2\pi n}{N}$. The subscript '$d$' on the amplitude of the complex beamforming weight, $w(\phi'_n)$, at the n^{th} antenna array element, denotes a discrete array.

The main difference between conventional beamforming with a continuous aperture versus a discrete array is that an array can only adjust the signal phase and amplitude across the antenna at the set of finite, discrete sampled locations. The phase, $\psi(\phi'_n)$, that maximizes the radiated field at (d_0, θ_0, ϕ_0) by ensuring that the product of exponentials has maximum value of one for all of the terms in the summation, is

$$\psi(\phi'_n) = kR\sin\theta_0\cos(\phi'_n-\phi_0) \tag{5.12}$$

With this phase, the radiated field from a transmitting antenna array with conventional beamforming, evaluated at any location in the farfield, (d, θ, ϕ), is

$$U(d,\theta,\phi) = \frac{a_d}{j\lambda}\frac{\exp(jkd)}{d}\sum_{n=0}^{N-1}\exp\left(jkR\sin\theta_0\cos(\phi'_n-\phi_0)\right)\exp\left(-jkR\sin\theta\cos(\phi'_n-\phi)\right)$$

(5.13)

Recall that, under conventional beamforming, the amplitude a_d is uniform across all of the elements. Thus, each array element transmits an equal fraction of the total power, which is limited.

Specifically, the total radiated power from the antenna array must satisfy the same power constraint as in the case of a transmitting aperture, namely $P_{rad} \le P_{tot}$. From (4.5), the total radiated power for the antenna array is

$$\begin{aligned} P_{rad} &= \int_0^{2\pi}\int_0^{2\pi}\left|U(d,\theta,\phi)\right|^2 d^2\sin\theta d\phi d\theta \\ &= \frac{a_d^2}{\lambda^2}\int_0^{2\pi}\int_0^{2\pi}\left|\sum_{n=0}^{N-1}\exp\left(jkR\sin\theta_0\cos(\phi'_n-\phi_0)\right)\exp\left(-jkR\sin\theta\cos(\phi'_n-\phi)\right)\right|^2\sin\theta d\phi d\theta \\ &= \frac{a_d^2}{\lambda^2}\int_0^{2\pi}\int_0^{2\pi}\left|F_d(\theta,\phi)\right|^2\sin\theta d\phi d\theta \end{aligned}$$

(5.14)

The quantity inside the absolute value in (5.14) is the discrete array factor, F_d (5.15).

$$F_d(\theta,\phi) = \sum_{n=0}^{N-1}\exp\left(jkR\sin\theta_0\cos(\phi'_n-\phi_0)\right)\exp\left(-jkR\sin\theta\cos(\phi'_n-\phi)\right) \quad (5.15)$$

Applying the power constraint on the transmitting antenna, we see that the array field amplitude, a_d, must satisfy (5.16).

$$a_d^2 \le \frac{P_{tot}\lambda^2}{\int_0^{2\pi}\int_0^{2\pi}|F_d(\theta,\phi)|^2 \sin\theta d\phi d\theta} \tag{5.16}$$

From (4.7) and with the discrete array factor in (5.15), the achievable antenna array directivity under the conventional beamforming scheme described by (5.11) is

$$\begin{aligned} D_{Array} &= \frac{4\pi|U(d_0,\theta_0,\phi_0)|^2}{\int_0^{2\pi}\int_0^{2\pi}|U(d,\theta,\phi)|^2 \sin\theta d\phi d\theta} \\ &= \frac{4\pi|F_d(\theta_0,\phi_0)|^2}{\int_0^{2\pi}\int_0^{2\pi}|F_d(\theta,\phi)|^2 \sin\theta d\phi d\theta} \\ &= \frac{4\pi N^2}{\int_0^{2\pi}\int_0^{2\pi}|F_d(\theta,\phi)|^2 \sin\theta d\phi d\theta} \end{aligned} \tag{5.17}$$

Like the aperture directivity in (5.9), the expression for the circular array directivity in (5.17) also has no simple closed form. We will now show calculations of the array directivity from Matlab and compare the results to that of an aperture. Note from the previous discussion on spatial sampling of an aperture, we expect that, with increasing number of antenna elements, the radiated array field should approach that of an aperture of the same size, since the former is simply a discrete version of the latter.

5.2.1 UCAA Directivity

In Fig. 5.1., we plot the array directivity (5.17) for UCAAs of different diameters as a function of the number of antenna elements N. First, note that the array directivity for a given antenna size and carrier wavelength remains constant when increasing N beyond a certain point, N_{sat}. Thus, in the limit as the number of elements approaches infinity, the aperture directivity is the same as that of an array with "large enough" element density. Moreover, examining the curves in Fig 5.1, we find that the UCAA directivity is approximately proportional to N up to a point. In the following discussion, we will determine the number of elements, N_{sat}, beyond which the array directivity remains constant.

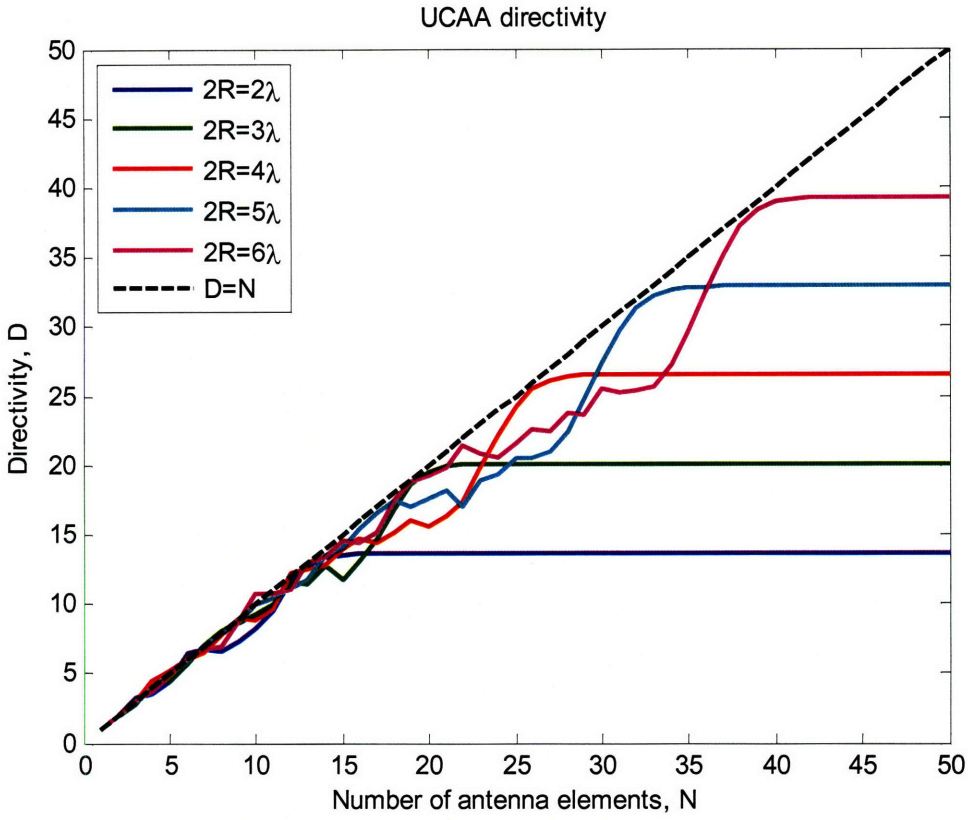

Fig. 5.1. UCAA Directivity versus the number of antenna elements for different antenna sizes.

In Fig. 5.2, we plot the maximum directivity of each curve in Fig. 5.1 as a function of the ratio of the array diameter, $2R$, to transmit wavelength λ.

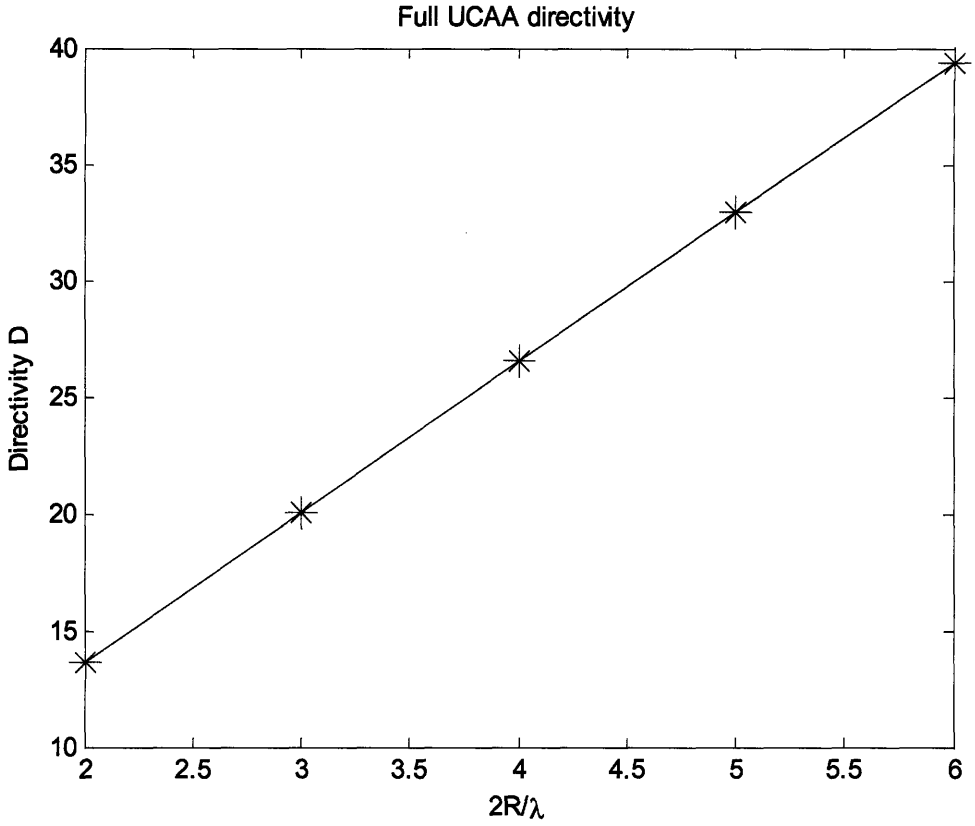

Fig. 5.2. Maximum Array Directivity as a function of the ratio of antenna size to carrier wavelength, $2R/\lambda$. The '*' represents computed directivity for the different ratios.

From this figure, we see that the maximum achievable directivity of a UCAA is approximately linearly proportional to the ratio $\frac{2R}{\lambda}$. Specifically, this maximum directivity is approximately 2π times the ratio $\frac{2R}{\lambda}$. From this analysis of maximum directivity, we find that N_{sat} is proportional to $\frac{4\pi R}{\lambda}$. Since N_{sat} must necessarily be an integer, we approximate this point of saturation as

$$N_{sat} \cong \left\lceil \frac{4\pi R}{\lambda} \right\rceil = \left\lceil \frac{2\pi R}{(\lambda/2)} \right\rceil \tag{5.18}$$

From (5.18), we see that the integer N_{sat} corresponds to element spacing of approximately $\lambda/2$ along the array circumference, $2\pi R$. From a sampling standpoint, N_{sat} is the number of UCAA elements required to sample the corresponding ring aperture at the spatial Nyquist sampling rate [21]. With this approximation in (5.18) and noting from Fig. 5.1 that the array directivity is approximately linear with N up to the point of saturation, N_{sat}, we have the array directivity D_{Array}:

$$D_{Array} \cong \begin{cases} N, & \text{for } N \le N_{sat} \\ N_{sat}, & \text{otherwise} \end{cases} \tag{5.19}$$

Fig. 5.3 plots the UCAA directivity for the same parameters plotted in Fig. 5.1, with our linear approximation (5.19) shown with dashed lines, and with the values of N_{sat} from (5.18) indicated by a star (*). From this figure, we see that our approximation to the UCAA directivity closely follows the calculated curves in Fig. 5.1.

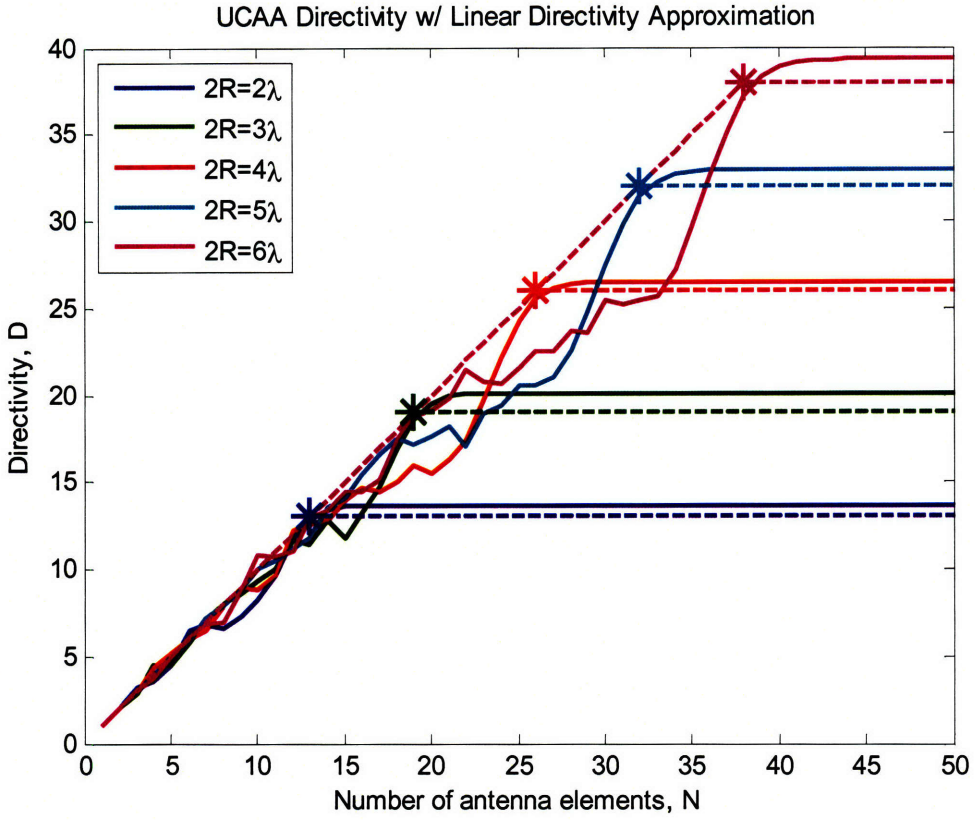

Fig. 5.3. Calculated UCAA directivity (5.17, solid), with linear approximation (5.19, dashed). N_{sat} indicated with a star '*'.

Since the array directivity is approximately proportional to the number of array elements, it takes on integer values in (5.19). A continuous aperture, on the other hand, does not have a discrete, integer number of elements. Thus, we can approximate $D_{Aperture}$ directly as

$$D_{Aperture} \cong \frac{4\pi R}{\lambda} \tag{5.20}$$

Fig. 5.4 plots the maximum achievable directivity as a function of $\frac{2R}{\lambda}$, as seen in Fig. 5.2, with the approximation to N_{sat} in (5.19) shown in red and the aperture

directivity approximation (5.20) in black. In Fig. 5.4 and Fig. 5.5, we see that our approximations to the UCAA directivity and points of saturation closely follow the calculated trends. We will use these approximations throughout the remainder of this thesis in order to simplify the integral equations in the previous section, allowing us to later offer insight into the behavior of data rates in the network without extensive calculations and simulations.

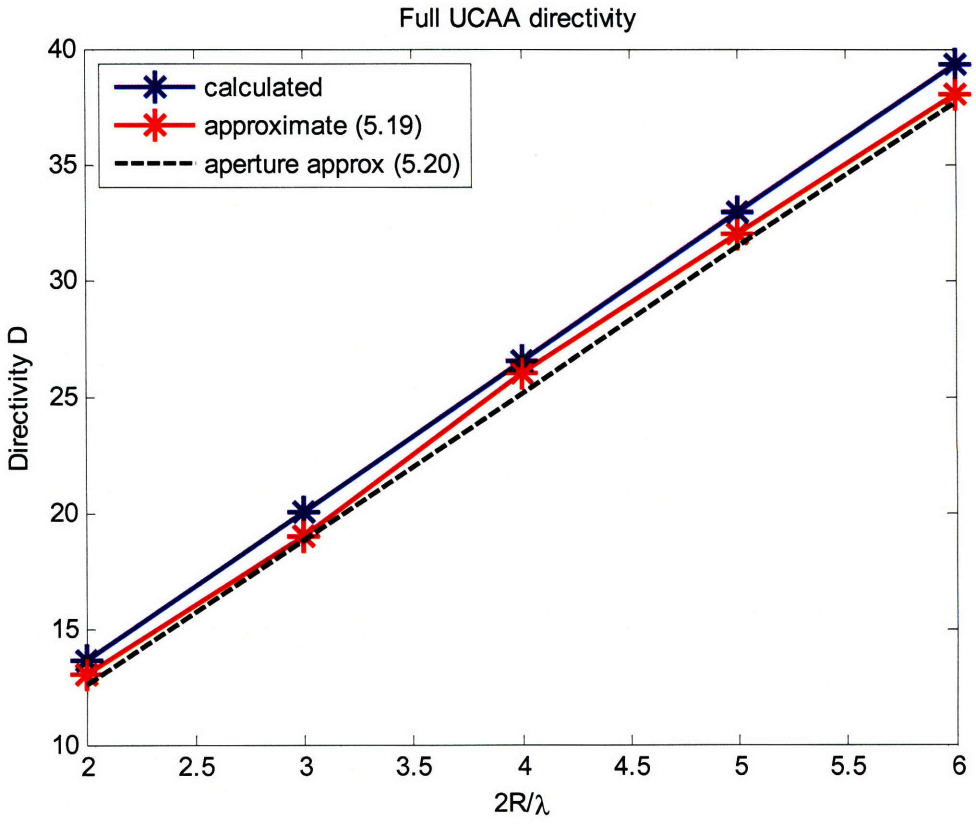

Fig. 5.4. Maximum UCAA directivity, calculated (blue) and approximated (red) as a function of the ratio of antenna size to carrier wavelength, $2R/\lambda$. Our approximation to the aperture directivity is shown in black (dashed).

5.2.2 Aperture & Array Beamforming Revisited

Following the directivity analysis in Matlab, we can now revisit aperture and array beamforming using our approximations in (5.18)-(5.20). With the array directivity in (5.19) that is proportional to N, the denominator in (5.17) becomes $4\pi N$ for $N \le N_{sat}$:

$$\int_0^{2\pi}\int_0^{2\pi} \left|F_d(\theta,\phi)\right|^2 \sin\theta d\phi d\theta \cong 4\pi N \tag{5.21}$$

Similarly, from (5.20), the denominator in (5.9) is given by

$$\int_0^{2\pi}\int_0^{2\pi} \left|F_c(\theta,\phi)\right|^2 \sin\theta d\phi d\theta \cong (2\pi)^2 \frac{\lambda}{R} \tag{5.22}$$

Using these values in (5.21) and (5.22), from (5.8) and (5.16), the maximum amplitudes on the aperture and array transmit fields, a_c and a_d, that satisfy the power constraint are:

$$a_c \cong \frac{1}{2\pi}\sqrt{\frac{P_{tot}\lambda}{R}} \tag{5.23}$$

$$a_d \cong \begin{cases} \sqrt{\dfrac{P_{tot}\lambda^2}{4\pi N}}, & \text{for } N \le N_{sat} \\ \sqrt{\dfrac{P_{tot}\lambda^2}{4\pi N_{sat}}} & \text{otherwise} \end{cases} \tag{5.24}$$

The user receive power will be determined by $|U(d_0,\theta_0,\phi_0)|^2$. From the above analysis of the directivity and complex weights of a UCAA utilizing conventional beamforming, this is equal to

$$|U(d_0,\theta_0,\phi_0)|^2 \cong \begin{cases} \dfrac{(2\pi)^2 R^2 a_c^2}{\lambda^2 d_0^2} = \dfrac{P_{tot}}{d_0^2}\dfrac{R}{\lambda} = \dfrac{D_{Aperture}P_{tot}}{4\pi d_0^2}, & Aperture \\ \dfrac{N^2 a_d^2}{\lambda^2 d_0^2} = \dfrac{NP_{tot}}{4\pi d_0^2} = \dfrac{D_{Array}P_{tot}}{4\pi d_0^2}, & Array \end{cases} \tag{5.25}$$

Note that, in terms of the aperture and array directivities defined in (5.19) and (5.20), the final expressions for the magnitude squared receive field due to a transmitting aperture and array are equivalent.

5.3 Receive Beamforming

Up to this point in this chapter, we have focused on beamforming for a transmitting aperture and array. We will now describe the dual receive beamforming problem. Recall that we are operating under a far-field assumption, so that the transmitted field at the receive aperture or array is well approximated by a plane wave. For the receive beamforming analysis, consider a circular antenna centered at the origin. Let this circular antenna now receive an incoming plane wave from a transmitting user located at (d_0,θ_0,ϕ_0).

On the receive end, the plane wave signal arriving at the antenna elements is scaled by complex beamforming weights and then summed to get the overall receive

power. From [21], the complex phase on a receiving antenna array, $\psi_r(\phi'_n)$, that maximizes the receive power from a user transmitting at (d_0, θ_0, ϕ_0) is given by

$$\psi_r(\phi'_n) = -kR\sin\theta_0\cos(\phi'_n - \phi_0) = -\psi(\phi'_n) \tag{5.26}$$

From (5.26), we see that the transmit and receive beamforming problems are symmetrical.

Unlike transmit antenna beamforming, the amplitude of the complex receive beamforming weights is not limited by the constraint on total time-averaged radiated power. In this thesis, we choose to normalize the receive beam, as in [21], such that the maximum receive gain is one and the gain in all other directions is less than unity. Thus, the amplitude on the receiving antenna array elements is $\frac{1}{N}$. Given this amplitude and the phase in (5.24), the complex weight, $w_r(\phi'_n)$, on the n^{th} element of a UCAA under a conventional beamforming scheme is given by (5.27).

$$w_r(\phi'_n) = \frac{1}{N}\exp\left(-jkR\sin\theta_0\cos(\phi'_n - \phi_0)\right) \tag{5.27}$$

Now that we have described conventional beamforming on both the transmitting and receiving ends of a single wireless link, we can extend our results to the case of transmitting simultaneously to multiple users from an individual antenna array.

5.4 Beamforming & Power Allocation for Multiple User Transmissions

Before considering beamforming and power allocation for simultaneous transmissions from a single antenna to M-1 users, we first outline the assumptions on the user signals sent over the wireless links. The information transmitted in the infrastructureless wireless network lies in the time-varying waveforms that each antenna element transmits. The signal transmitted to user j is the time-varying waveform $v_j(t)$. Following the discussion of the user signals in [1], we assume that the user signals $v_j(t)$ are independent of each other and their individual time-averaged value, $\bar{v}_j(t)$, is zero (5.28) but the time-averaged magnitude squared of each signal, $\left|v_j(t)\right|^2$, is unity (5.29).

$$\bar{v}_j(t) = 0 \tag{5.28}$$

$$\overline{\left|v_j(t)\right|^2} = 1 \tag{5.29}$$

Furthermore, we assume that different user signals are uncorrelated:

$$\overline{v_j(t)v_k^*(t)} = 0, k \neq j \tag{5.30}$$

With these assumptions on user signals at the transmit antenna array, we can superimpose multiple beams directed towards spatially distributed users. More specifically, given these signal properties, the beams for distinct user signals will not distort each other and the amplitude and phase at the antenna elements decouple for different user transmissions. Thus, beamforming for multiple simultaneous user

transmissions at a single antenna array is simply a superposition of the beams formed for each user transmission. Moreover, due to the assumption that user signals are uncorrelated, the total radiated power is the sum of the power radiated by each of these beams, which is constrained by the limitation on total time-averaged transmit power from an individual antenna.

At an individual antenna array element, each user transmission is given a distinct complex weight. The complex weights for each of the M-1 simultaneous user transmissions are determined by (5.12). The amplitude on each set of complex weights is determined to satisfy the overall power constraint. That is, each user transmission is allocated a fraction α_j of the total available power, P_{tot}, at an individual antenna, where $0 \leq \alpha_j \leq 1$. Hence, the sum of all of the α_j terms for $M-1$ user transmissions from a single antenna must be less than or equal to one (5.31).

$$\sum_{j=1}^{M-1} \alpha_j \leq 1 \tag{5.31}$$

With this power allocation scheme, the limitation on power for each individual transmission from a particular antenna becomes $\alpha_j P_{tot}$. From (5.22), the corresponding amplitude on the complex antenna array element weights for a particular user transmission is then

$$a_j = \sqrt{\frac{\alpha_j P_{tot} \lambda^2}{4\pi N}} \tag{5.32}$$

With this amplitude, the magnitude squared of field received at user j, located at (d_0, θ_0, ϕ_0), from an individual transmitting antenna is

$$\left|U_j(d_0,\theta_0,\phi_0)\right|^2 = \frac{N\alpha_j P_{tot}}{4\pi d_0^2} = \frac{D_{Array}\alpha_j P_{tot}}{4\pi d_0^2} \tag{5.33}$$

For a network of M wireless users, the power allocation scheme described above is applied at each transmitting user antenna. The fraction of total power allocated by user i to a transmission to user j, α_{ij}, will determine the receive power at user j on this individual link. With normalized maximum receive gain, the receive power at user j due to a transmission from user i is then

$$P_{ij} = \frac{N\alpha_{ij} P_{tot}}{4\pi d_0^2} \tag{5.34}$$

On the other hand, the power allocated to other wireless links will determine the levels of interference received at user j. From (3.1), we see that the achievable data rate on a wireless link formed by user i transmitting to user j is determined by the receive power and interference at user j. Thus, the α's in the power allocation scheme for the network will determine the achievable data rates.

The power allocation scheme described above can be summarized for the entire wireless network in the power allocation matrix shown in (5.35). Each α_{ij} term in the matrix specifies the power allocation on the wireless link formed by user i transmitting to

user j. The diagonal in the power allocation matrix is zero to indicate that there are no self-transmissions. Also, from (5.29), the sum of the entries in each row of the power allocation matrix must be less than or equal to one.

Power Allocation Matrix

$$\begin{bmatrix} 0 & \alpha_{12} & \alpha_{13} & \dots & \alpha_{1M} \\ \alpha_{21} & 0 & \alpha_{23} & \dots & \\ \alpha_{31} & \alpha_{32} & 0 & & \\ \dots & \dots & & \dots & \\ \alpha_{M1} & & & & 0 \end{bmatrix} \tag{5.35}$$

As discussed above, the power allocation scheme specified by the matrix shown in Fig. 5.5 will determine the achievable data rates on individual wireless links in the network. The problem of joint beamforming and power allocation to achieve a desired traffic pattern in a network considers solving for the α's in the matrix above in order to satisfy the user data rate demands. Due to the interference terms that link the power allocation and achievable data rates for different users, determining the power allocation scheme to satisfy a given traffic pattern for a network with a large number of users can be difficult. To get a sense of the network problem, we will consider power allocation and examine achievable data rates for a simple network of three users.

Chapter 6

Beam Characteristics, Sidelobe Behavior, and Interference in the Wireless Network

Multiple simultaneous transmissions, as discussed in Chapter 5, cause interference in a wireless network. The amount of interference at a user is determined by the amount of power allocated to interfering transmissions and the transmit and receive gains between user pairs. In Chapter 5, we examined the maximum directive gain of a beam formed by conventional beamforming at a UCAA. In order to find the amount of interference at a user, we need to examine the directive gain of an antenna in all directions. This chapter will focus on the beampattern of a UCAA in order to characterize the mutual interferences of multiple transmissions in an infrastructureless wireless network.

6.1 Beampattern and Beamwidth

Since the users in our wireless problem transmit and receive on the *x*-*y* plane (i.e. $\theta = \pi/2$), we are only concerned with the antenna directive gain as a function of ϕ. An example beampattern for a UCAA with radius $R = \lambda$ and N_{sat} elements is shown in Fig. 6.1, which plots the directive gains (normalized by the directivity) versus ϕ. The complex weights of the UCAA are chosen such that the maximum directive gain is in the $\phi_0 = \frac{\pi}{2}$ direction. The beam pointing in the ϕ_0 direction is called the *mainbeam*. Outside

of the mainbeam, there are *sidelobes* and *nulls*. Sidelobes are the secondary peaks and nulls are points at which the directive gains are zero.

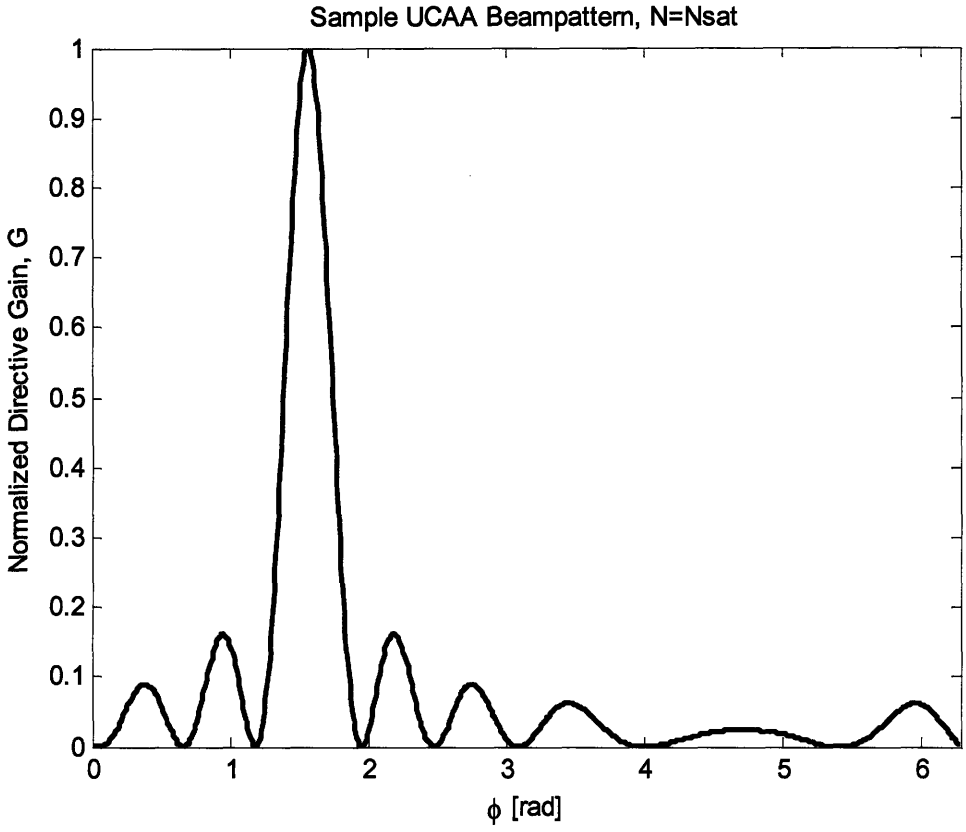

Fig. 6.1. Beampattern for a UCAA of radius $R = \lambda$ with N_{sat} elements.

An important parameter in characterizing the mainbeam is the *beamwidth*. This angular beam width is typically measured between points along the mainbeam that are 3dB lower than the directivity, as shown in Fig. 6.2. One can also define the beamwidth by other dB values such as 10dB or 15dB as indicated by Fig. 6.2. The beamwidth is proportional to $\frac{\lambda}{2R}$ and, subsequently, we will take the mainbeam width to be $\lambda/2R$ [19].

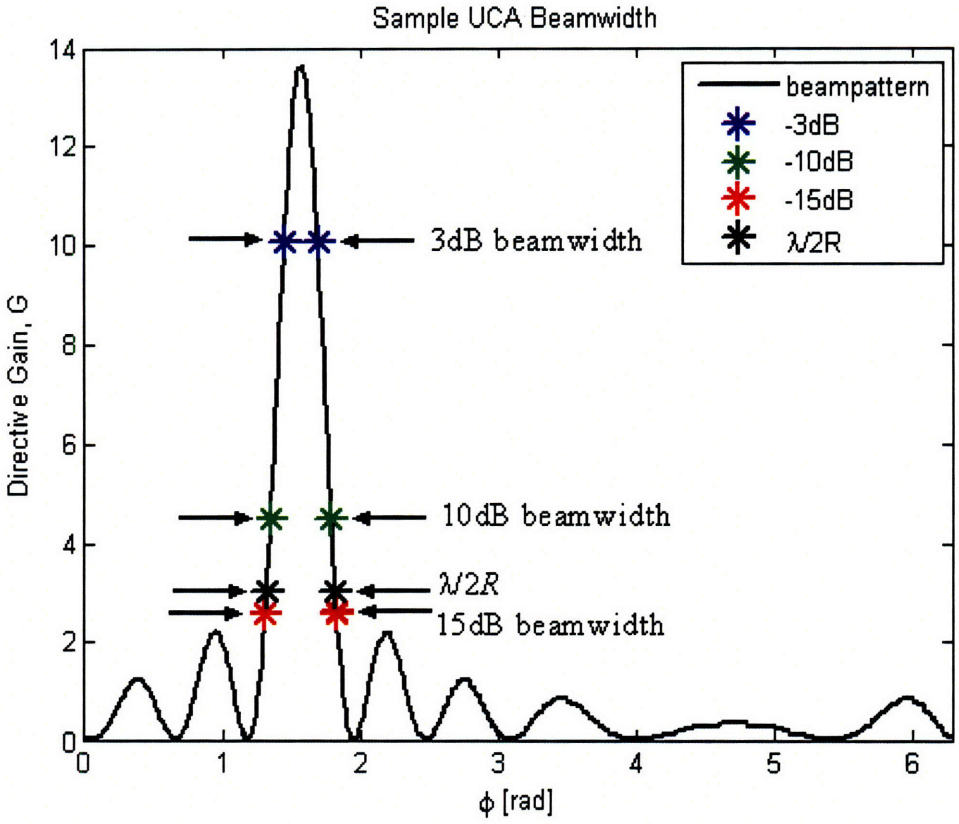

Fig. 6.2. Sample UCAA beampattern with 3dB, 10dB, 15dB and $\lambda/2R$ beamwidths.

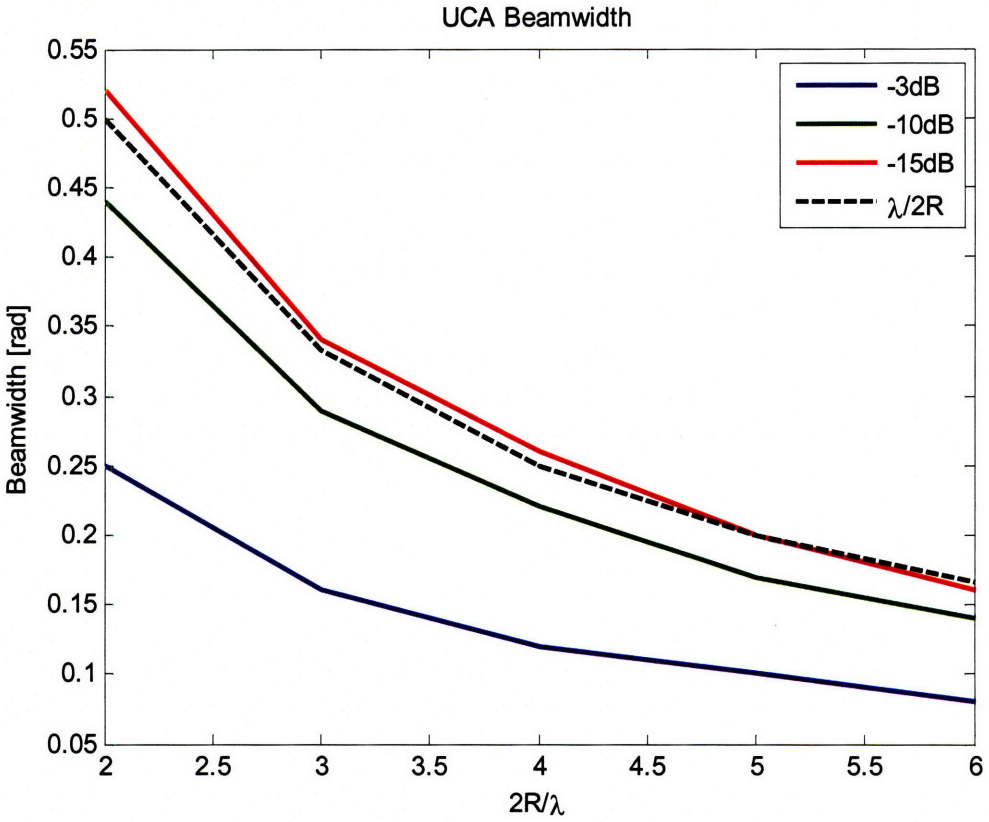

Fig. 6.3. UCAA beamwidth as a function of the ratio of antenna diameters to carrier wavelength, $2R/\lambda$.

Fig. 6.4 shows polar plots of the beampattern for two different arrays with different diameters. In these plots, as expected, the mainbeam beamwidth is smaller for the larger array, indicating that larger arrays can focus more power in the desired direction. In general, the beampattern of an antenna depends not only on the antenna diameter, but also on the number of antenna elements as we will show next.

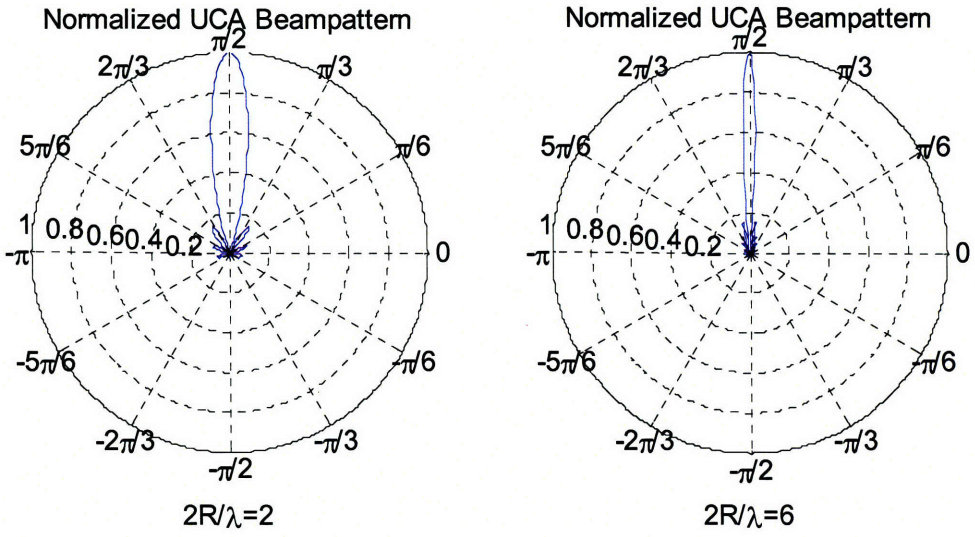

Fig. 6.4. Comparison of UCAA beamwidths for two different ratios of antenna diameter to carrier wavelength (normalized polar beam plots).

6.2 Spatial Aliasing in the UCAA Beampattern

Recall from Chapter 5 that the UCAA directivity does not change for $N > N_{sat}$. Similarly, from our study in Matlab, we find that the beampattern does not change significantly for $N > N_{sat}$. Consequently, in the remainder of this chapter we consider UCAAs with $N \leq N_{sat}$ elements.

A UCAA with $N < N_{sat}$ elements is spatially sampled below the Nyquist rate (i.e. undersampled) which causes spatial aliasing in the UCAA beampattern. That is, the beampattern for an under-sampled UCAA will contain *grating lobes*, or spatially aliased sidelobes. Fig. 6.5 shows polar plots of the beampatterns of a UCAA with radius $R = \lambda$ and $N \leq N_{sat}$. The beampatterns in these plots are normalized by the directivity.

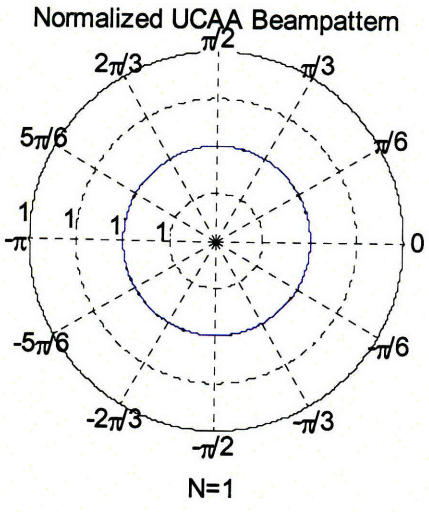

N=1

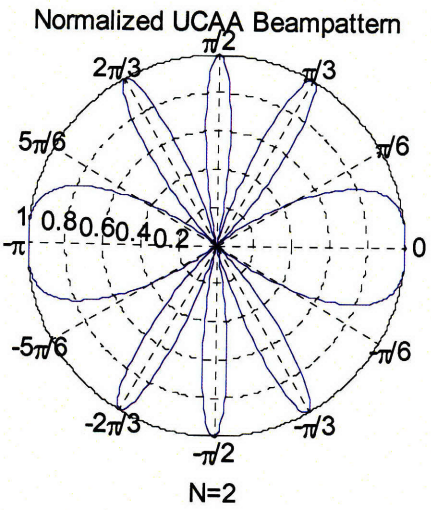

N=2

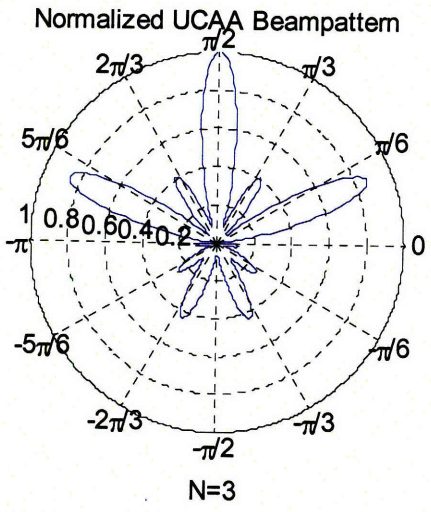

N=3

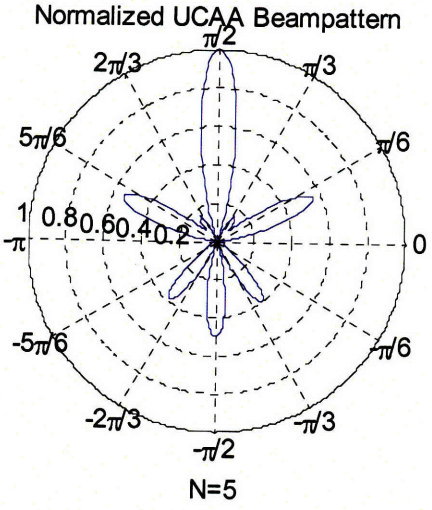

N=5

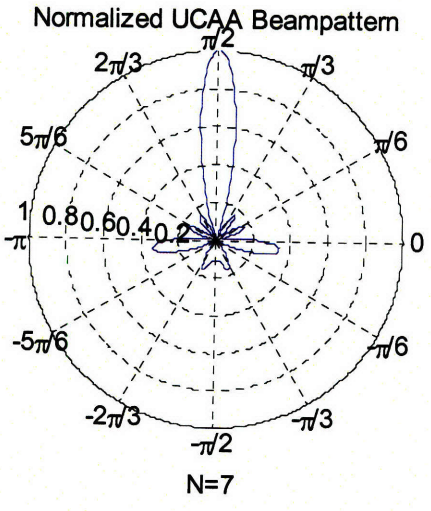

N=7

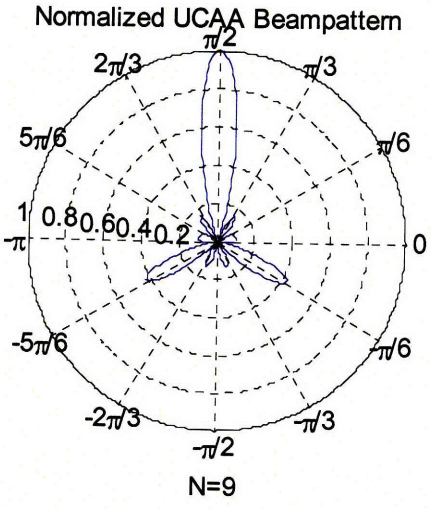

N=9

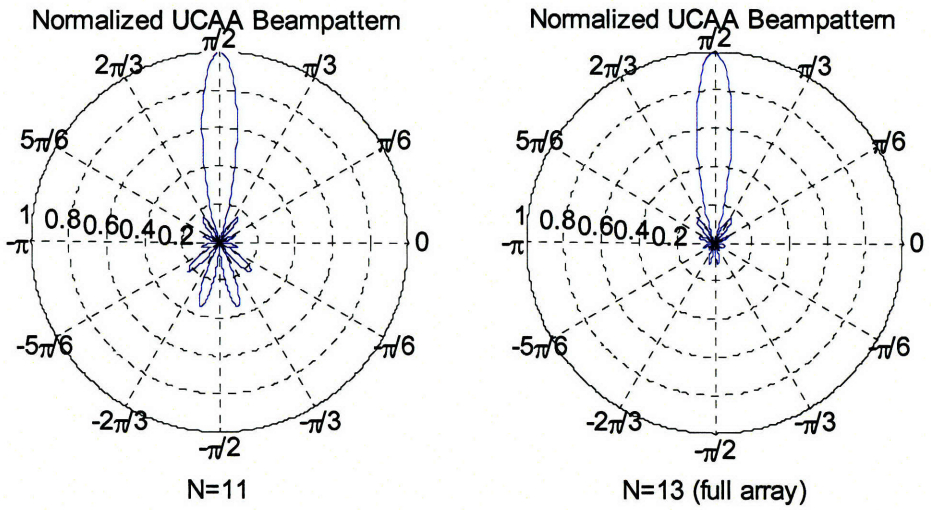

Fig. 6.5. Polar beam plots: $N_{sat} = 13, 2R/\lambda = 2, \phi_0 = \frac{\pi}{2}$.

Comparing the spatially aliased beampatterns in Fig. 6.5 to that of a "full" array in the last plot of Fig. 6.5, we note that the sidelobes in the beampattern for a full array are much lower than the grating lobes of the under-sampled UCAAs. Moreover, as is evident in Fig. 6.1, the sidelobes for a full array decay in amplitude with increasing angle away from the mainbeam, whereas the grating lobes do not always decrease.

To see the variability in grating lobe locations for a range of under-sampled arrays, we plot the beampattern for a UCAA of radius 3λ as a function of N and ϕ in Fig. 6.6. We see that the directivity of these arrays (in $\phi_0 = \frac{\pi}{2}$ direction) grows linearly with N and saturates at $N = N_{sat}$, as described in Chapter 5. Outside of the mainbeams, we observe grating lobes that vary significantly in amplitude and location as a function of N and ϕ. These properties of grating lobes for UCAAs indicate that the interference gains in a network can vary significantly with user location and number of antenna elements N.

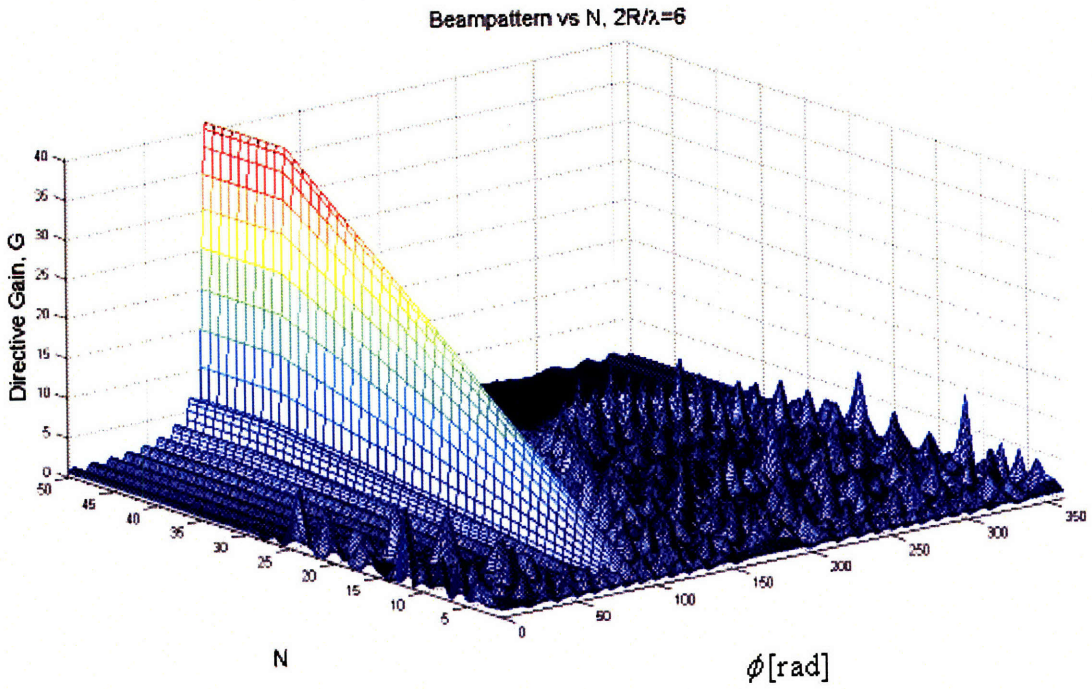

Fig. 6.6. UCAA beampattern as a function of N, $N_{sat} = 40, 2R/\lambda = 6, \phi_0 = \frac{\pi}{2}$.

6.3 Sidelobe levels of a UCAA Beampattern

The sidelobe levels of the antenna transmit and receive beams will determine the amount of interference that users in a network will experience. Consequently, the precise level of interference at a receiver depends on the exact user locations. Calculation of these interference levels directly from (4.7), for each possible user location, is computationally intensive, particularly, if the nodes are not static. Meaningful analysis of the wireless channels therefore requires some simplification and parameterization of the sidelobes and, correspondingly, interference levels. For our goal of gaining insight into the achievable data rates of infrastructureless wireless networks, we make

approximations to the sidelobe levels in order to find an expression for the data rate on an individual wireless link that is independent of the precise user locations. Specifically, we determine the minimum, maximum and average sidelobe levels of a UCAA as a function of the density of antenna array elements in order to provide insight into the best, worst and average performances in the infrastructureless network, respectively.

In particular, we define the maximum (minimum respectively) sidelobe level as the ratio of the maximum (minimum respectively) gain outside of the mainbeam to the directivity. Similarly, the average sidelobe level is the ratio of the average value of the sidelobes to the directivity. To find the average value of the sidelobes, we integrate the beampattern outside of the mainbeam (specified by the beamwidth $\frac{\lambda}{2R}$) and divide by $2\pi - \frac{\lambda}{2R}$. We will express the sidelobe levels as a fraction, ζ, that lies between zero, for a null, and one, corresponding to the directivity. Moreover, we express ζ as a function of N/N_{sat}, a term that indicates the density of antenna elements, or sparsity of the array.

6.3.1 Maximum Sidelobe Level

The maximum sidelobe level describes the largest gain on interfering transmissions and therefore captures the worst case performance in the wireless network. We attempt to find a curve that envelopes most of the UCAA maximum sidelobe levels as a function of N/N_{sat}. From numerical computation, we find that ζ_{max} is 0.16 for $N = N_{sat}$, as shown in the beampattern for a full array in Fig. 6.1. With this observation and

examination of the UCAA maximum sidelobe levels in Matlab, we make the approximation to the UCAA maximum sidelobe level, ζ_{max}:

$$\zeta_{\max} = 1.16 - N/N_{sat} \tag{6.1}$$

Fig. 6.7 plots the maximum sidelobe level of beampatterns of UCAAs of different relative sizes as a function of N/N_{sat}. Our enveloping approximation to the UCAA maximum sidelobe level is shown on this plot in black and, as is evident in Fig 6.7, captures the trends of the maximum sidelobe levels.

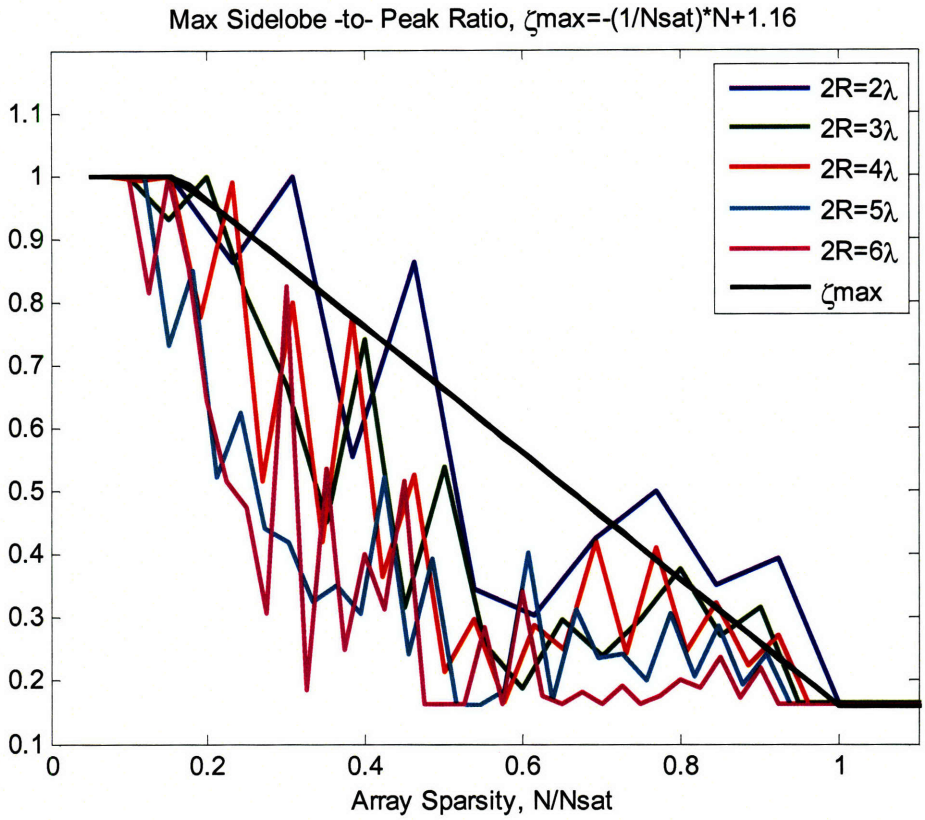

Fig. 6.7. Ratio of Maximum Sidelobe-to-Peak UCAA beam level as a function of array sparsity N/N_{sat}, shown with the approximation $\zeta_{\max} = 1.16 - N/N_{sat}$ (black).

To see the individual curves in Fig. 6.7 more clearly, we show plots of the calculated (blue) and approximate (green) maximum sidelobe levels in Fig. 6.8 for each relative UCAA size. As is evident in Fig. 6.8, our approximation, $\zeta_{\max}$, lies on the calculated curves for smaller UCAAs and envelopes, or offers a more conservative estimate, of the sidelobe levels for larger UCAAs.

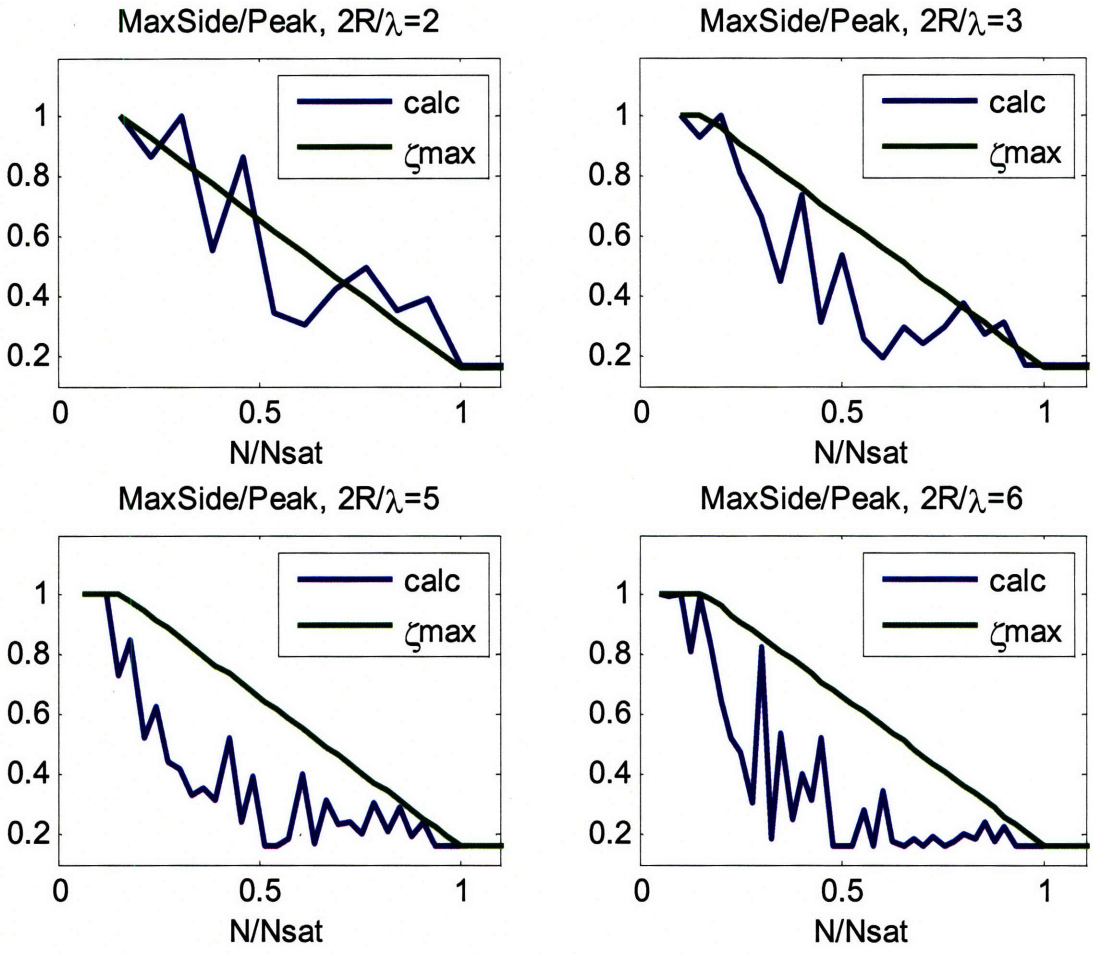

Fig. 6.8. Plots of the ratio of Maximum Sidelobe-to-Peak UCAA beam level as a function of array sparsity N/N_{sat} for different ratios of antenna size to carrier wavelength. Plots shown with the approximation $\zeta_{\max} = 1.16 - N/N_{sat}$ (green).

6.3.2 Average Sidelobe Level

The average sidelobe level characterizes the average interference in the network. Upon examination of the average sidelobe level for multiple ratios of array diameter to wavelength, we find that ζ_{ave} is approximately $1/N$ (6.2). Fig. 6.9 plots the average

sidelobe level as a function of N/N_{sat} for different ratios, $\frac{2R}{\lambda}$, with our approximations from (6.2) shown with dashed lines. We have also shown this plot on a dB scale in Fig. 6.10. As is evident in Fig. 6.9 and Fig. 6.10, our approximation closely follows the trend in average sidelobe levels among the UCAAs of different relative sizes.

$$\zeta_{ave} = 1/N \tag{6.2}$$

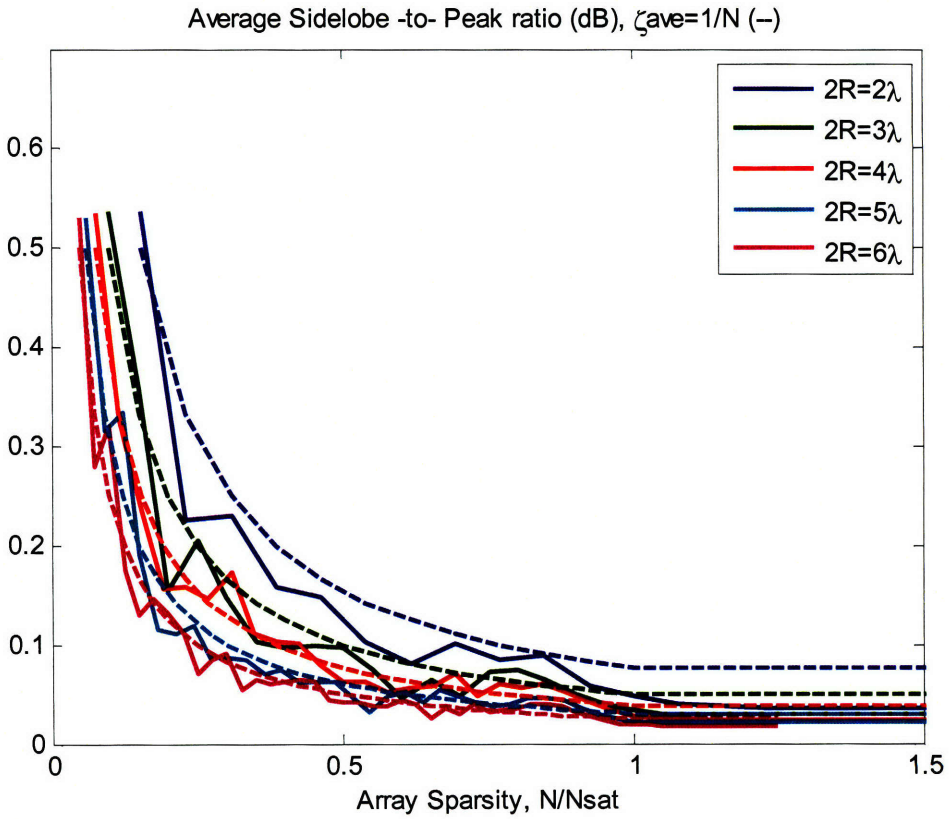

Fig. 6.9. Ratio of Average Sidelobe-to-Peak UCAA beam level as a function of array sparsity N/N_{sat} (linear scale), shown with the approximation $\zeta_{ave} = 1/N$ (dashed).

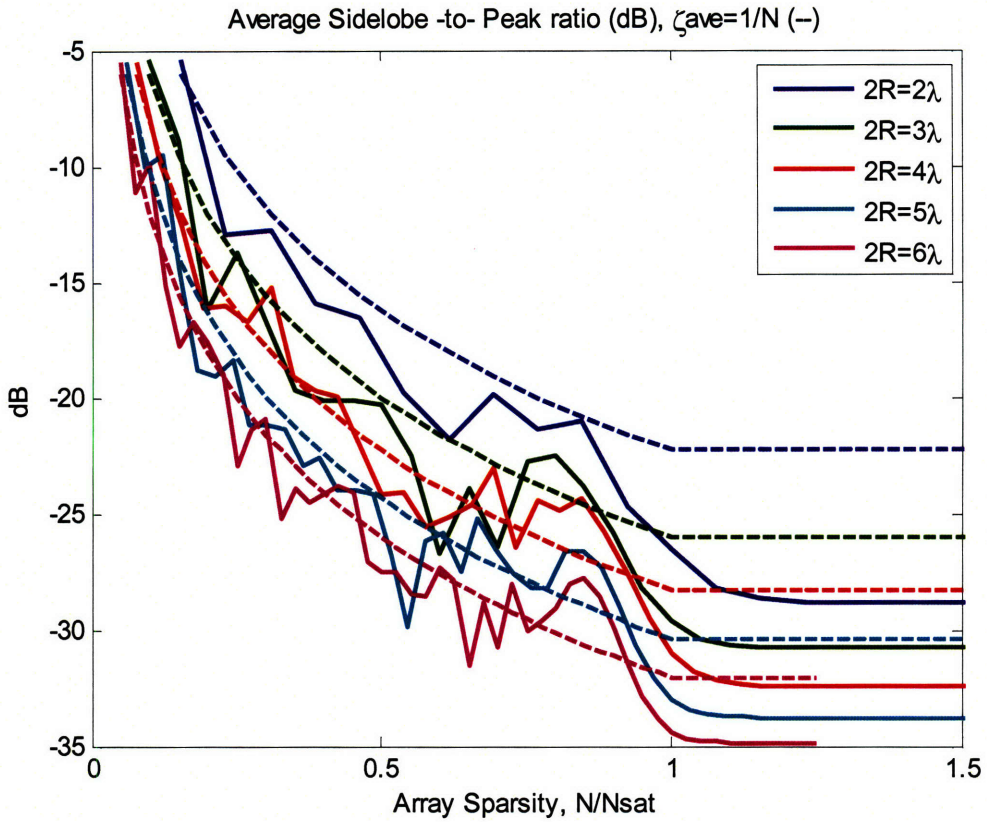

Fig. 6.10. Ratio of Average Sidelobe-to-Peak UCAA beam level as a function of array sparsity N/N_{sat} (dB scale), shown with the approximation $\zeta_{ave} = 1/N$ (dashed).

To see the individual curves in Fig. 6.9 and Fig. 6.10 more clearly, we show plots of the calculated (blue) and approximate (green) average sidelobe levels in Fig. 6.11 and Fig. 6.12 for each relative UCAA size. In these figures, our approximation, ζ_{ave}, follows the calculated curves of UCAA average sidelobe levels. At N_{sat}, our approximation provides a conservative estimate of the average sidelobe level.

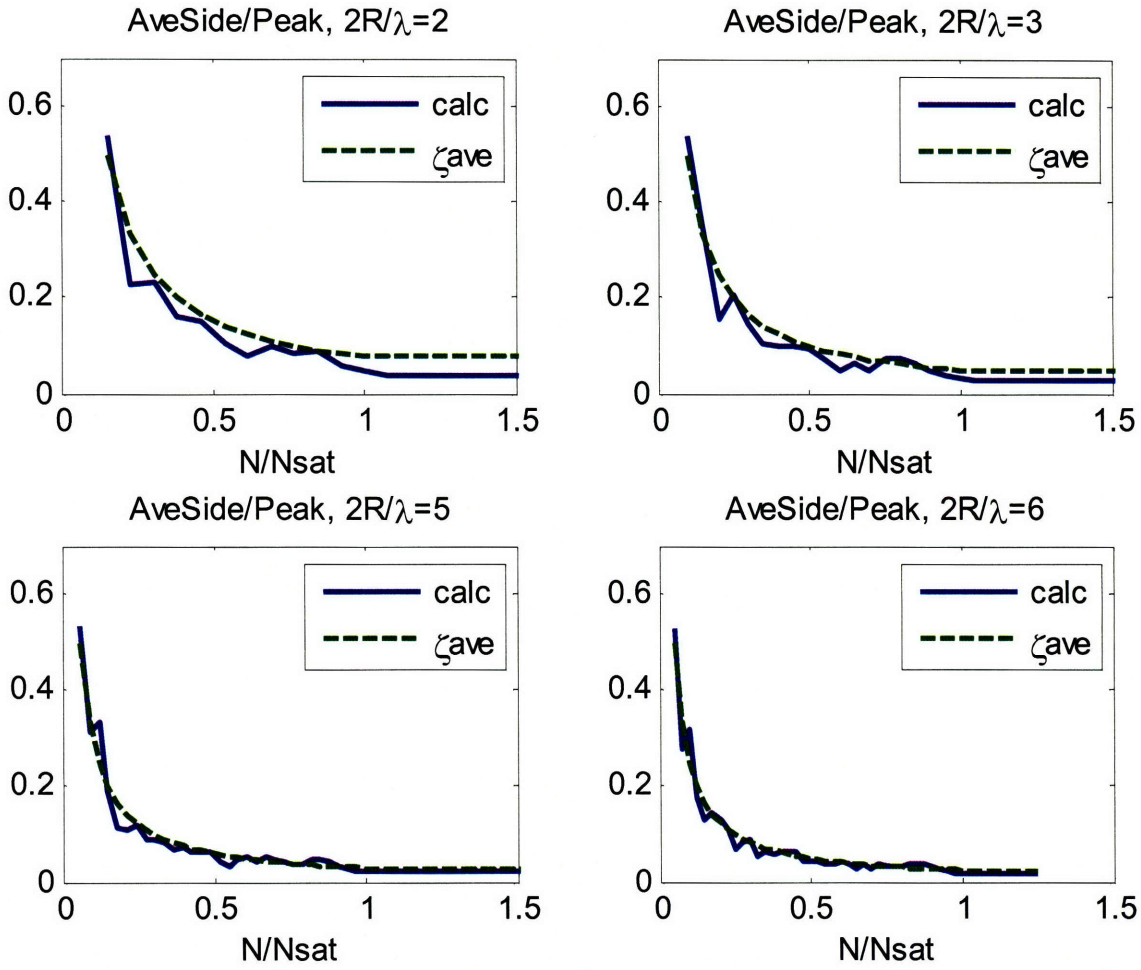

Fig. 6.11. Plots of the ratio of Average Sidelobe-to-Peak UCAA beam level as a function of array sparsity N/N_{sat} for different ratios of antenna size to carrier wavelength. Plots shown with the approximation $\zeta_{ave} = 1/N$ (dashed green).

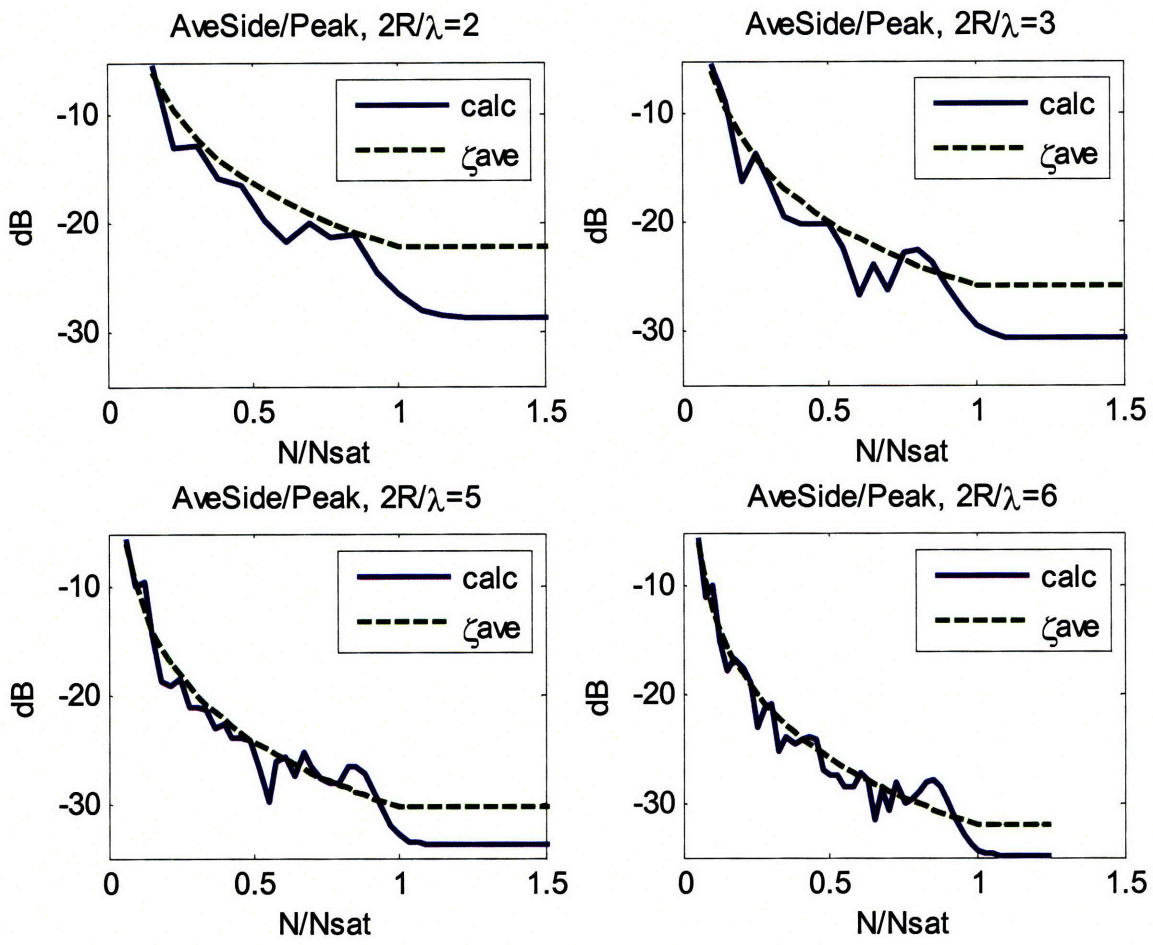

Fig. 6.12. Plots of the ratio of Average Sidelobe-to-Peak UCAA beam level (dB scale) as a function of array sparsity N/N_{sat} for different ratios of antenna size to carrier wavelength. Plots shown with the approximation $\zeta_{ave} = 1/N$ (dashed green).

6.3.3 Minimum Sidelobe Level

The minimum sidelobe level corresponds to locations in a null. For a location in the null of interfering transmissions, $\zeta_{\min} = 0$, and there is no interference. Therefore, this scenario upper bounds the performance of the wireless network.

6.4 Beam Parameter Summary

Table 6-1 summarizes the beampattern results analyzed in this chapter including directivity, beamwidth and sidelobe levels parameterized by N, λ and R.

Table 6-1. UCAA beamparameter summary.

Beam Parameters $N \leq N_{sat}$	
Directivity	N
Beamwidth	$\lambda/2R$
Max Sidelobe	$\zeta_{\max} = 1.16 - N/N_{sat}$
Ave Sidelobe	$\zeta_{ave} = 1/N$
Min Sidelobe	$\zeta_{\min} = 0$

6.5 Receive Interference

Following the beampattern characterization in the previous sections, we are now able to analyze interference in the wireless network. As discussed in Chapter 5, a single antenna can transmit simultaneously to multiple users, forming separate beams for each transmission. Our work considers scenarios in which transmissions from an individual antenna have non-overlapping mainbeams (specified by the beamwidth). The work in [1]

shows that scheduling users transmissions with overlapping mainbeams in different time slots offers considerable benefit over transmitting to these users simultaneously. We assume that these scenarios can be scheduled appropriately and therefore focus our attention on the case of transmitting with non-overlapping mainbeams.

For the following analysis of interference in a wireless channel, consider the wireless link formed by user *i* transmitting to user *j*. This link is represented by the index (*i,j*), indicating the particular transmit-receive pair. Let the set of users be denoted by P. Let $k \in \mathrm{P}, k \neq i, j$, and $l \in \mathrm{P}, l \neq k, i, j$. Assuming no self-interference, interfering transmissions on the (*i,j*) link are from (*i,k*), (*k,j*), and (*k,l*). Utilizing our notation for sidelobe level, ζ, the transmit and receive gains (G^t and G^r) on these interfering transmissions are shown in Table 6-2. The total interference on a link is represented by a *G* with a subscript indicating the transmit-receive pair, that is the product of the transmit and receive gains on the link.

Table 6-2 Interference gains.

Desired Transmission: i→j			
Interference $\forall k,l$	Transmit Gain	Receive Gain	Total Gain
(*i,k*)	$G_{ik}^t = \zeta N$	$G_{ik}^r = 1$	$G_{ik} = \zeta N$
(*k,l*)	$G_{kl}^t = \zeta N$	$G_{kl}^r = \zeta$	$G_{kl} = \zeta^2 N$
(*k,j*)	$G_{kj}^t = N$	$G_{kj}^r = \zeta$	$G_{kj} = \zeta N$

With the assumption that user signals are uncorrelated and have unit time-averaged power outlined in (5.27) and (5.28), the total interference received at user j on the (i,j) link is simply the sum of the power received from each of the (i,k), (k,j), and (k,l) transmissions among the M network users.

$$I_{tot} \cong \zeta \frac{NP_{tot}}{4\pi} \sum_{\substack{k=1 \\ k \neq i,j}}^{M-2} \sum_{\substack{l=1 \\ l \neq k}}^{M-2} \left(\frac{\alpha_{ik}}{d_{ik}^2} + \frac{\zeta \alpha_{kl}}{d_{kl}^2} + \frac{\alpha_{kj}}{d_{kj}^2} \right) \tag{6.3}$$

Chapter 7

Achievable Data Rates for a Three-User Network

In this chapter, we examine achievable data rates in a wireless network, as a function of the number of antenna elements, with varying noise power and interference. In order to isolate the effects of these parameters on data rates in a network, we consider a simple network of three users located at the vertices of an equilateral triangle. First, based on our beamforming and interference analyses, we examine the user data rate on an individual link in this network with all users transmitting to each other simultaneously at all times. Second, we consider scheduling of user transmissions at different times in this simple network. In particular, we compare the achievable user data rates for three scheduling schemes with varying N for different levels of noise power and interference.

7.1 User Data Rate

The simple three-user network that we consider is shown in Fig. 7.1. In this network, the users are all separated by a distance d and each user is equipped with an N-element UCAA. Recall from Chapter 6 that, if $N > N_{sat}$, the antenna beampattern for a UCAA does not change significantly with increasing number of elements; thus, we consider network performance for $N \leq N_{sat}$. As a first-order study, we assume a uniform traffic pattern whereby each user transmits at the same rate, on average, to the other two users. In total, there are six pairwise transmissions.

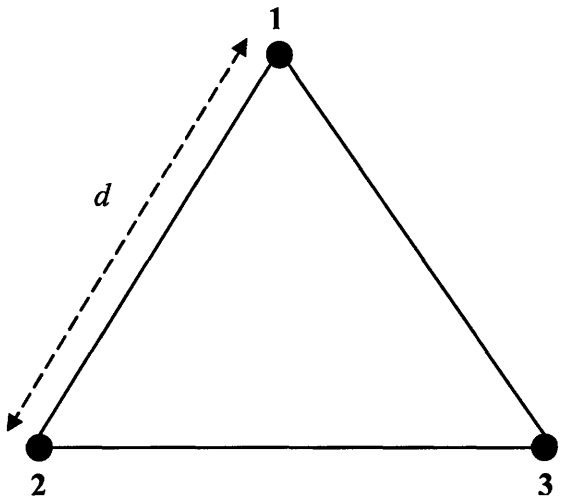

Fig. 7.1. Three Node Network.

With each user transmitting at the same rate to all users at all times and with all user pairs separated by the same distance, d, each pairwise transmission is allocated the same fraction of power, and $\alpha_{ij} = \alpha_{kl} = \alpha_{ik}, \forall i, j, k, l$. In this case, consider a pairwise transmission from user i to user j. With the symmetrical network topology shown in Fig. 7.1, the receive power (5.34) at user j from user i's transmission can be approximated (see Chapter 5) by

$$P_{ij}^{A} \cong \frac{\alpha_{ij} N P_{tot}}{4\pi d^2} \tag{7.1}$$

With all of the α's equal, from (6.3), the received interference at user j, I_{ij}^{A}, is approximately

$$I_{ij}^{A} \cong \alpha_{ij}\zeta N\frac{P_{tot}}{4\pi d^2}(2+\zeta) \tag{7.2}$$

$$\text{where } \zeta = \begin{cases} 0, & \min \\ \frac{1}{N}, & \text{ave} \\ 1.16-\frac{N}{N_{sat}}, & \max \end{cases}$$

Combining (7.2), (7.3), and the noise power N_0W, where N_0 is the noise power density in units of power per unit bandwidth, and W is the channel bandwidth, the SINR on link (i,j) is approximately

$$\text{SINR}_{ij}^{A} \cong \frac{P_{ij}^{A}}{N_0W + I_{ij}^{A}} = \frac{\alpha_{ij}\frac{NP_{tot}}{4\pi d^2}}{N_0W + \alpha_{ij}\zeta N\frac{P_{tot}}{4\pi d^2}(2+\zeta)} \tag{7.3}$$

From (3.1), we see that the data rate on link (i,j) is equal to $W\log_2(1+\text{SINR}_{ij})$, thus, the α_{ij} that maximizes the SINR will maximize the data rate. From (7.4), we find that the SINR_{ij} as a function of α_{ij} is concave down. Therefore, we chose the largest possible α_{ij} to maximize the common data rate. Under our constraint that $\sum_{j=1}^{M-1}\alpha_{ij} \le 1$, we find that $\alpha_{ij} = \frac{1}{2}$ for our simple network. That is, to maximize the common data rate, each user transmits at the full average power of P_{tot}, with half of P_{tot} allocated for transmission to each of the destination users. The power allocation matrix for this case with simultaneous transmissions and no user scheduling at different times (Scheme A) is:

$$
\begin{array}{cc} & \text{Rx} \\ & \begin{array}{ccc} 1 & 2 & 3 \end{array} \\ \text{Tx} \begin{array}{c} 1 \\ 2 \\ 3 \end{array} & \begin{bmatrix} 0 & 1/2 & 1/2 \\ 1/2 & 0 & 1/2 \\ 1/2 & 1/2 & 0 \end{bmatrix} \end{array} \tag{7.4}
$$

With this power allocation matrix, the data rate on link (i,j) for Scheme A is

$$
R_{ij}^{A} \cong W \log_2 \left(1 + \frac{\frac{NP_{tot}}{8\pi d^2}}{N_0 W + \zeta N \frac{P_{tot}}{4\pi d^2}\left(1+\frac{1}{2}\zeta\right)} \right) \tag{7.5}
$$

With expression (7.5), we can now analyze the achievable data rate for Scheme A under some special cases: (1) assuming zero interference, (2) high interference compared to noise power (interference-dominated), and (3) in the limit of large bandwidth. These special cases are useful for elucidating regions of operation where detailed antenna and interference modeling are important.

First, the achievable data rate assuming zero interference is determined from the signal-to-noise ratio (SNR). The data rate on link (i,j) is then

$$
\begin{aligned}
R_{ij}^{A} &\cong W\log_2(1+\mathrm{SNR}_{ij}^{A}),\ \text{assuming } I_{ij}^{A}=0 \\
&= W\log_2\left(1+\frac{NP_{tot}}{8\pi d^2 N_0 W}\right)
\end{aligned}
\tag{7.6}
$$

Since interference is assumed to be zero, simultaneous transmission for all user pairs will strictly outperform any other user scheduling scheme. Hence, this data rate is the highest achievable data rate for the three-user network under the uniform traffic pattern. Practically, this scenario corresponds to a special case where users are located in antenna beampattern nulls of other users.

With nonzero interference and relatively low noise power (ie. interference-dominated) the SINR can be approximated by the signal-to-interference ratio (SIR). This yields

$$
\begin{aligned}
R_{ij}^{A} &\cong W\log_2(1+\mathrm{SIR}_{ij}^{A}),\ \text{assuming interference-dominated} \\
&= W\log_2\left(1+\frac{P_{ij}^{A}}{I_{ij}^{A}}\right) \\
&= W\log_2\left(1+\frac{1}{\zeta\left(1+\frac{1}{2}\zeta\right)}\right)
\end{aligned}
\tag{7.7}
$$

Finally, consider the noise dominated regime where interference is nonzero but is much smaller than the noise power. This occurs either when bandwidth W and/or noise power density N_0 is large. The pairwise data rate goes to zero as $N_0 \to \infty$, however, the rate is finite as $W \to \infty$. From here, we examine the achievable data rate in the large

bandwidth limit. The noise-dominated data rate on link (i,j) is shown in (7.8) with the limit as the bandwidth approaches infinity below.

$$\begin{aligned} R_{ij}^{A} &\cong W\log_2\left(1+\frac{NP_{tot}}{8\pi d^2 N_0 W}\right), \text{ assuming noise - dominated} \\ &\cong \frac{NP_{tot}}{\ln(2)8\pi d^2 N_0}, \text{ assuming } W\to\infty \end{aligned} \tag{7.8}$$

The rate in the large bandwidth limit results from the approximation that $\ln(1+x)\approx x$ for $x<<1$.

Clearly, the relative levels of interference and noise power have significant impacts on the user data rate as can be seen by comparing (7.6)-(7.8). To further illustrate this, we plot (7.5) in Figure 7.2 for transmit and receive UCAAs of radius $\frac{3\lambda}{2}$, $N = 10$ elements (ie. N_{sat} = 19), $\frac{P_{tot}}{4\pi d^2}=1\left[\mathrm{W}/\mathrm{m}^2\right]$ and channel bandwidth W=10^6 Hz under minimum, maximum and average interference levels (I_{min}, I_{max}, I_{ave}) as a function of the noise power density, N_0. In the low noise power density regime (interference-dominated), it can be seen that the pairwise data rate approaches that of (7.7).

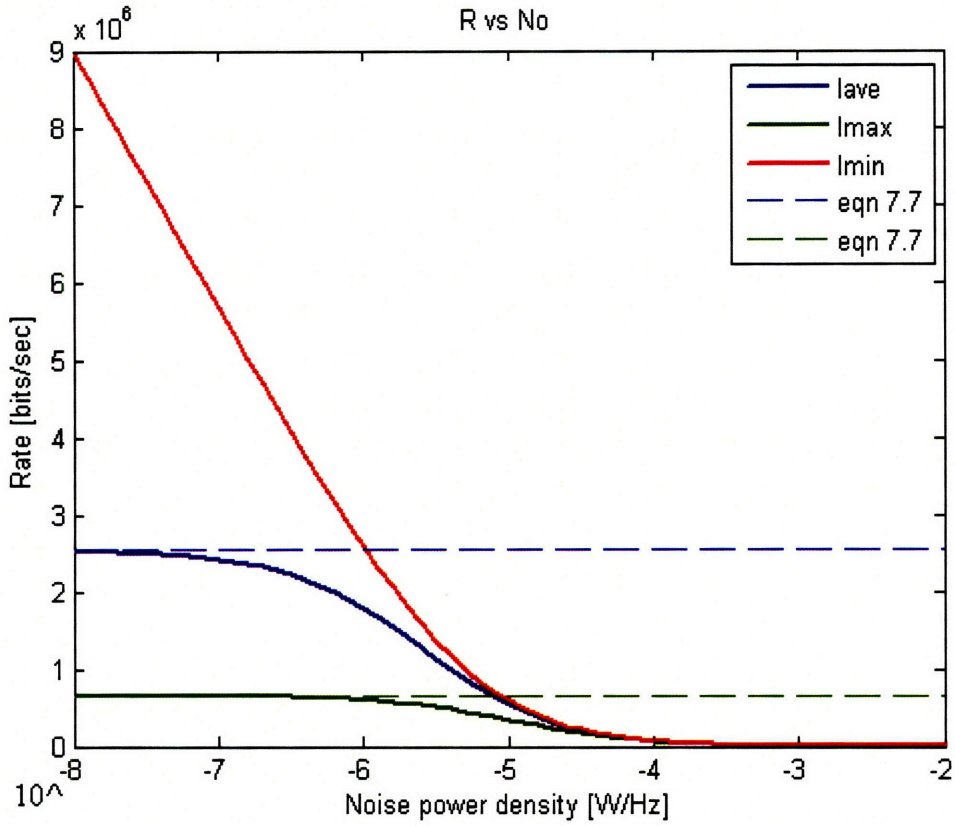

Fig. 7.2. User data rates under Scheme A without scheduling for minimum, average and maximum interference as a function of noise power density, $\frac{P_{tot}}{4\pi d^2} = 1\left[\mathrm{W}/\mathrm{m}^2\right]$.

As can be seen from Fig 7.2, in regions with relatively high noise power density, the three rate curves converge. Since noise dominates in this region, detailed interference modeling is unnecessary. In regions with relatively low noise power density, however, the difference in data rates under minimum, maximum and average interference can be significant. In this region then, a user located in antenna beampattern nulls of other users can achieve significantly higher data rates than a user located in the direction of antenna sidelobes of other users. Consequently, using the maximum interference may yield very conservative estimates of the achievable data rate while using the minimum interference may yield overly optimistic results. These bounds on the data rate are therefore only

useful for first-order analytical studies. To obtain the exact data rate, one can use the detailed expressions in Chapters 4 and 5.

In addition to the level of noise power in relation to interference, we examine how the pairwise data rate varies with the number of antenna array elements. Generally, with increasing N, the data rate in (7.5) will increase due to increased directivity up to N_{sat}, at which point, further increase in the number of antenna elements does not increase the data rate. Table 7-1 shows how the interference-dominated rate and the rate in the large bandwidth limit vary with N, for $N \leq N_{sat}$. First, the interference-dominated rate is determined by the SIR, as indicated in (7.7). In this case, recall from Chapter 6 that the sidelobe levels on interfering transmissions decrease with increasing N, so the SIR and corresponding rate increase, as shown in the first row of Table 10-1. Second, in the large bandwidth limit, the achievable data rates for all levels of interference are linear with N. Thus, from the analysis in this section and the results in Table 7-1, we find that the achievable user data rate on a wireless link increases with increasing N ($N \leq N_{sat}$) for all levels of noise power and interference.

Table 7-1. Interference-dominated and large bandwidth rates as a function of N.

	Rate with varying N
Interference-Dominated	$R \propto \log_2(N)$, (I_{ave}) $R \propto \log_2(N_{sat}) - \frac{1}{\log_2(N)}$, $(I_{\max})$
Large Bandwidth Limit	$R \propto N$

Fig. 7.3 illustrates how the data rates under Scheme A vary with N for different channel bandwidths. This representative plot uses the same parameters as in Fig. 7.2, but with fixed noise power density at $N_0 = 10^{-3}\left[\mathrm{W}/\mathrm{Hz}\right]$ and varying channel bandwidth and number of antenna elements.

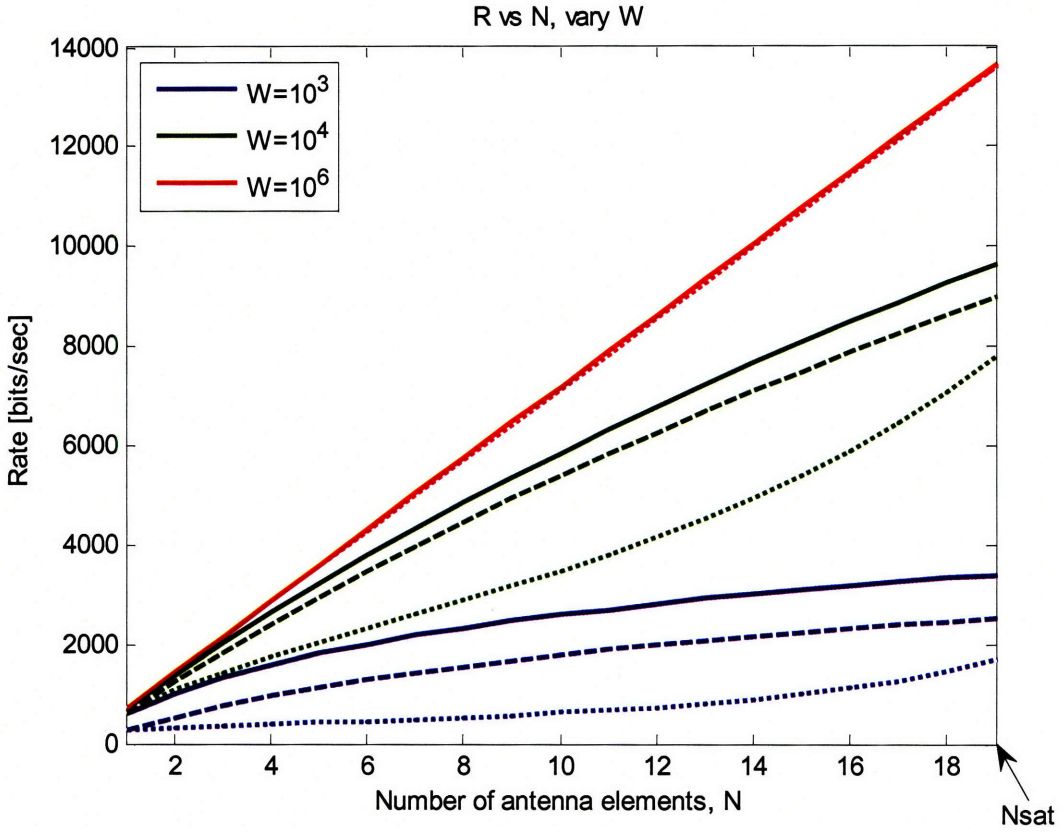

Fig. 7.3. Rate versus the number of antenna elements with varying bandwidth for I_{min} (solid), I_{ave} (dashed) & I_{max} (dotted), $\frac{P_{tot}}{4\pi d^2} = 1\left[\mathrm{W}/\mathrm{m}^2\right]$ (N_{sat}=19).

Fig. 7.3 shows that the number of antenna elements at the transmit and receive UCAAs has a significant effect on the achievable data rates. In the best case, the pairwise data rate increases linearly with N (corresponding to the large bandwidth limit) and

saturates for $N > N_{sat}$. As bandwidth decreases, the pairwise data rate becomes increasingly interference-limited and increases sub-linearly with N. Depending on the number of antenna elements, the gap between the pairwise data rate under I_{min} and I_{max} changes as well, highlighting again the importance of detailed interference modeling in some cases. Again, we stress again that all of these rate curves in this representative plot remain constant for $N > N_{sat}$.

7.2 Data Rates with User Scheduling

From our examination of the pairwise data rate in our simple network without scheduling, we found that the rate behavior varies significantly as a function of the number of antenna elements and, in the interference-dominated regime, for different levels of interference. In this section, we extend our analysis to consider scheduling user transmissions at different times, thereby eliminating sources of interference in the network. In particular, we consider two scheduling schemes utilizing time-sharing, or scheduling user transmissions at different times, in our equilateral triangle network shown in Fig. 7.1. We examine the achievable data rates for these schemes with time-sharing for zero interference, in the interference-dominant case, and in the large bandwidth limit, so that we can compare these rates with those discussed previously for the network without scheduling.

The first scheduling scheme with time-sharing divides time into equal duration slots. In the first time slots, each of the six pairwise transmissions is assigned a unique slot. This transmission assignment is then repeated for all subsequent time slots, giving each pairwise transmission one slot of transmission time in every six time slots. Since

only a single transmission occurs in each time slot, there is no interference in the network. We call this scheduling scheme Scheme *B*. In order to maximize the common data rate and to satisfy the maximum average power constraint, each user transmits with an average power of $3P_{tot}$, when it is it's turn to transmit. It is easy to see that, averaged over time, each node transmits P_{tot} amount of power, which satisfies the maximum average power constraint. The approximate received power at user j from user i's transmission under Scheme *B* is then

$$P_{ij}^{B} \cong \frac{3NP_{tot}}{4\pi d^2} \tag{7.10}$$

Since each pairwise transmission transmits 1/6 of the time, the average receive data rate on the (i,j) link is given by

$$R_{ij}^{B} \cong \frac{1}{6} W \log_2\left(1+\frac{3NP_{tot}}{4\pi d^2 N_0 W}\right) \tag{7.11}$$

Scheme *B* eliminates all interference among the users, but, as is evident by the Signal-to-noise ration (SNR) in (7.11), the pairwise data rate under this scheme is sensitive to changes in noise power. In the large bandwidth limit, R_{ij}^{B} becomes

$$R_{ij}^{B} \cong \frac{NP_{tot}}{\ln(2)8\pi d^2 N_o}, \text{assuming } W \to \infty \tag{7.12}$$

Comparing (7.12) and (7.8), we find that, in the large bandwidth limit, the average data rate on link (i,j) under Schemes A and B are identical. For large W, interference is negligible, so both scheduling schemes simply amount to different ways of allocating equal power, on average in time, across all of the network links. Also, for very large bandwidth, one can allocate a fraction of bandwidth to each user transmission, so that, with this frequency division multiplexing (FDM) scheme, simultaneous user transmissions do not interfere with each other.

Now we consider another time-sharing scheme, Scheme C, in which only some of the sources of interference are eliminated. In particular, time is divided into equal duration slots as in Scheme B. In the first time slot, pairwise transmissions (1,2), (2,3), and (3,1) are scheduled. In the second time slot, pairwise transmissions (2,1), (3,2), and (1,3) are scheduled. This pattern is repeated for all subsequent time slots. This corresponds to users transmitting clockwise around the network in Fig. 7.1 half of the time, and counter-clockwise the other half. To maximize the common data rate for users in the network under Scheme C, each user transmits P_{tot} amount of power in each time slot. The approximate received power at user j from user i's transmission is

$$P_{ij}^{C} \cong \frac{NP_{tot}}{4\pi d^2} \tag{7.13}$$

Under Scheme C, interference due to the (i,k), (k,j) links in Table 6-2 are eliminated and only the interfering transmission with the smallest gain, (k,l), remains. The receive interference at user j is given by

$$I_{ij}^{C} \cong \zeta^2 N \frac{P_{tot}}{4\pi d^2} \tag{7.14}$$

Given the receive power and interference in (7.13) and (7.14), the receive data rate on link (i,j) is approximately

$$R_{ij}^{C} \cong \frac{1}{2} W \log_2 \left(1 + \frac{\frac{NP_{tot}}{4\pi d^2}}{N_0 W + \zeta^2 \frac{NP_{tot}}{4\pi d^2}} \right) \tag{7.15}$$

where the $\frac{1}{2}$ comes from scheduling transmissions over two time intervals.

Assuming zero interference, this rate becomes

$$\begin{aligned} R_{ij}^{C} &\cong \frac{1}{2} W \log_2 (1 + \mathrm{SNR}_{ij}^{C}), \text{ assuming } I_{ij}^{C} = 0 \\ &= \frac{1}{2} W \log_2 \left(1 + \frac{NP_{tot}}{4\pi d^2 N_0 W} \right) \end{aligned} \tag{7.16}$$

Comparing (7.16), (7.11) and (7.6), we find that, without interference, there is no clear benefit to scheduling user transmissions at different times. While the rates grow logarithmically (at best) with the SNRs for these schemes, the rates in (7.11) and (7.16) are scaled by a fraction resulting from time-averaging in the case of users transmitting in different time slots. We will examine this further in the next section when we compare the achievable data rates under the three schemes.

In the interference-dominated regime,

$$R_{ij}^{C} \cong \frac{1}{2} W \log_2\left(1+\frac{1}{\zeta^2}\right), \text{ Interference-dominated} \qquad (7.17)$$

where $\frac{1}{\zeta^2}$ is the SIR. In the next section, we will compare the data rates in (7.17) and (7.7) in the interference-dominated region and gain insight into when there is potential benefit to scheduling user transmissions in our network as in Scheme *C*.

Finally, in the large bandwidth limit, the rate in (7.15) becomes

$$R_{ij}^{C} \cong \frac{NP_{tot}}{\ln(2) 8\pi d^2 N_o}, \text{assuming } W \to \infty \qquad (7.18)$$

Comparing (7.18), (7.12), and (7.8), we see that, in the large bandwidth limit, the achievable user data rates are identical for all of the scheduling schemes *A*, *B*, and *C* in our network. This indicates that the differences between interference modeling and scheduling are negligible with large channel bandwidth. Recall, also, that with large bandwidth, FDM can eliminate interference among users in the network.

The following table shows the expressions for achievable pairwise data rates in our equilateral triangle network with the three different scheduling schemes, under the assumption of no interference, with interference dominating, and in the large bandwidth limit. Note that we do not exhaustively examine all possible scheduling schemes, but simply offer these three example schemes to gain an understanding of the potential benefits of different scheduling in our network.

Table 7-2. Summary of average user data rate for scheduling schemes *A*, *B*, and *C*.

	R^A	R^B	R^C
	$W\log_2\left(1+\frac{N\frac{P_{tot}}{8\pi d^2}}{N_0W+\zeta N\frac{P_{tot}}{4\pi d^2}\left(1+\frac{1}{2}\zeta\right)}\right)$	$\frac{1}{6}W\log_2\left(1+\frac{3NP_{tot}}{4\pi d^2N_0W}\right)$	$\frac{1}{2}W\log_2\left(1+\frac{\frac{NP_{tot}}{4\pi d^2}}{N_0W+\zeta^2\frac{NP_{tot}}{4\pi d^2}}\right)$
I=0	$W\log_2(1+\frac{NP_{tot}}{8\pi d^2N_0W})$	$\frac{1}{6}W\log_2\left(1+\frac{3NP_{tot}}{4\pi d^2N_0W}\right)$	$\frac{1}{2}W\log_2\left(1+\frac{NP_{tot}}{4\pi d^2N_0W}\right)$
Large W Limit	$\frac{NP_{tot}}{\ln(2)8\pi d^2N_o}$	$\frac{NP_{tot}}{\ln(2)8\pi d^2N_o}$	$\frac{NP_{tot}}{\ln(2)8\pi d^2N_o}$
Interference-Dominated	$W\log_2\left(1+\frac{1}{\zeta\left(1+\frac{1}{2}\zeta\right)}\right)$	$\frac{1}{6}W\log_2\left(1+\frac{3NP_{tot}}{4\pi d^2N_0W}\right)$ (no interference)	$\frac{1}{2}W\log_2\left(1+\frac{1}{\zeta^2}\right)$

7.3 Comparison of Average Data Rate for Scheduling Schemes *A*, *B* & *C*

In this section, we compare the achievable data rates under the three schemes that we have considered in order to examine the potential benefits of scheduling user transmissions at different times in our simple network. Specifically, we show representative plots of these data rates, as a function of the number of antenna elements, with varying noise power in relation to the interference. We find that, in certain cases, such as those with no interference or low noise compared to interference, some of the scheduling schemes clearly outperform the others. On the other hand, in the large bandwidth limit, all of the pairwise data rates behave identically, regardless of scheduling or interference, as indicated in Table 7-2. For more moderate levels of noise power in relation to interference, we find that no scheme dominates. In particular, the scheduling schemes yielding the highest data rates depend specifically on the interference modeling and number of antenna elements.

For the representative plots in this section, we plot the data rates in (7.5), (7.11) and (7.15) as a function of the number of antenna elements. We examine the minimum, average, and maximum interference levels, as specified by the functions, ζ, approximating the sidelobe levels. We consider the same parameters as in section 7.1, mainly: $R = \frac{3\lambda}{2}$; $\frac{P_{tot}}{4\pi d^2} = 1\left[\mathrm{W}/\mathrm{m}^2\right]$; W=10^6 Hz and $N_0 = 10^{-3}\left[\mathrm{W}/\mathrm{Hz}\right]$ and explicitly note when we vary any of these parameters in our representative plots.

First, assuming no interference, we find that the data rate transmitting to all users at the same time is the largest for all cases, with exception in the large bandwidth limit in

which all schemes yield identical rates. In Fig. 7.4, we plot the data rates under the different schemes assuming zero interference for varying noise power density. In these plots, scheme *A* (no scheduling of users at different times) clearly outperforms the others. Without interference, users can transmit to each other at all times without hurting the pairwise data rates, thus, there is no benefit to scheduling user transmissions at different times.

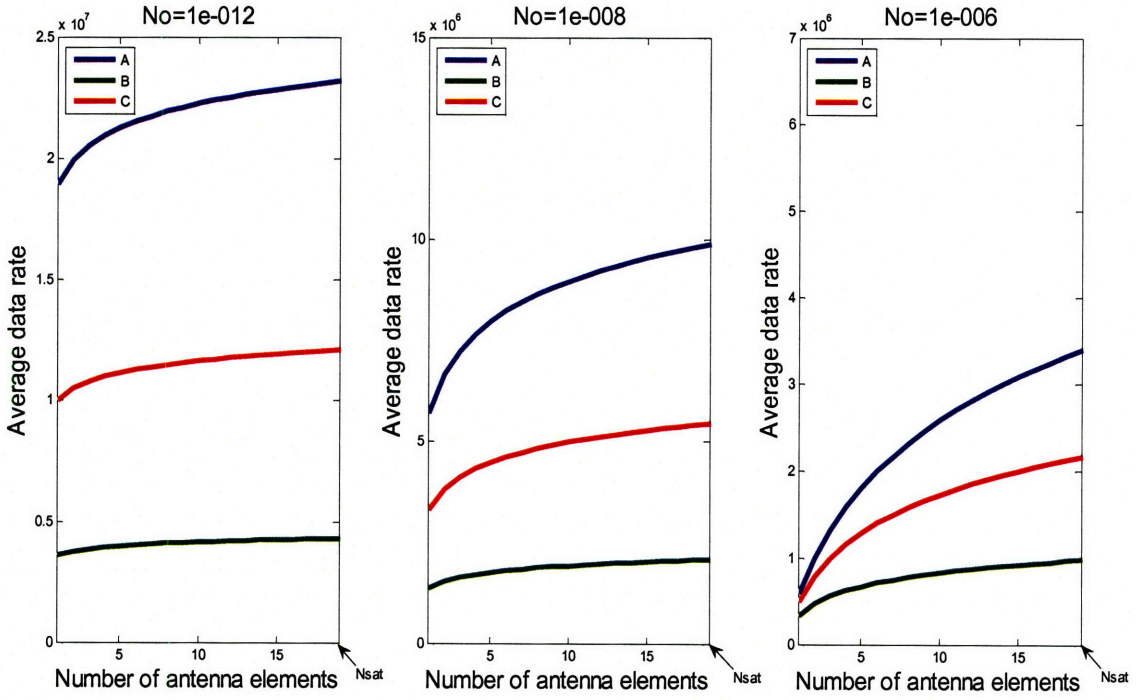

Fig. 7.4. Data rates as a function of the number of antenna elements for zero interference and varying noise power density $\frac{P_{tot}}{4\pi d^2} = 1\left[\mathrm{W}/\mathrm{m}^2\right]$, ($N_{sat}$=19).

Conversely, with nonzero interference and relatively low noise power (i.e. severely interference-dominated), scheduling user transmissions at different times offers the most benefit. While the scheduling schemes *A* and *C* yield interference-dominated

rates for this case, as shown in Table 7-2, the data rate resulting from the scheduling scheme *B* is determined by an SNR, which grows without bound as noise power decreases. Thus, in the severely interference-dominating case, scheme *B* yields the highest data rate, followed by scheme *C*. Fig. 7.5 plots the pairwise data rate under the different scheduling schemes with nonzero interference and relatively small noise power density ($N_0 = 10^{-8}\left[\mathrm{W/Hz}\right]$). It is evident from this plot that, for low noise relative to interference, scheduling user transmissions to eliminate interference in the network offers considerable benefit over transmitting simultaneously at all times.

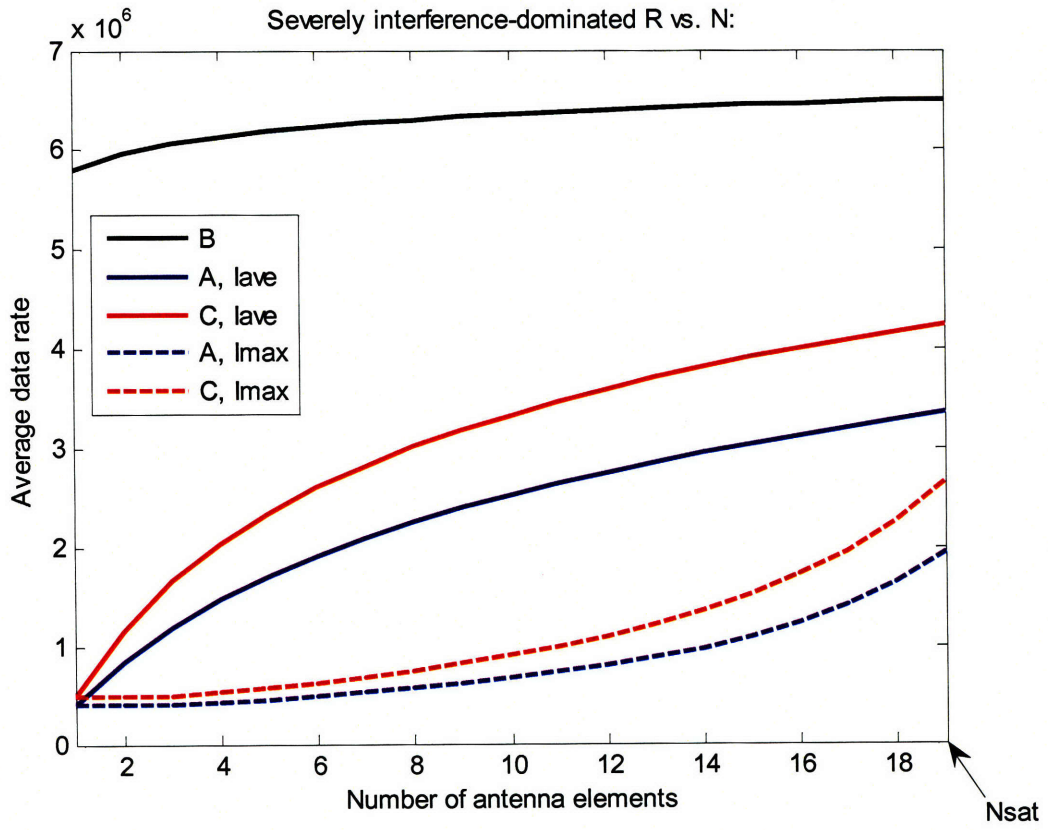

Fig. 7.5. Data rate as a function of the number of antenna elements for the severely interference-dominated case, $N_0 = 10^{-8}\left[\frac{\mathrm{W}}{\mathrm{m}^2}\right]$, $\frac{P_{tot}}{4\pi d^2} = 1\left[\mathrm{W/m^2}\right]$, ($N_{sat}$=19).

Unlike the cases of zero interference and nonzero interference with low noise power, in the large bandwidth limit, there is no difference between the achievable data rates for different scheduling schemes and levels of interference. This effect of increasing channel bandwidth is shown in Fig. 7.6, in which all of the rates become the same asymptotically for large W, as indicated in Table 7-2. That is, the differences between interference levels and scheduling schemes evident in the curves for lower bandwidths become negligible with increasing W and the rates grow linearly with N.

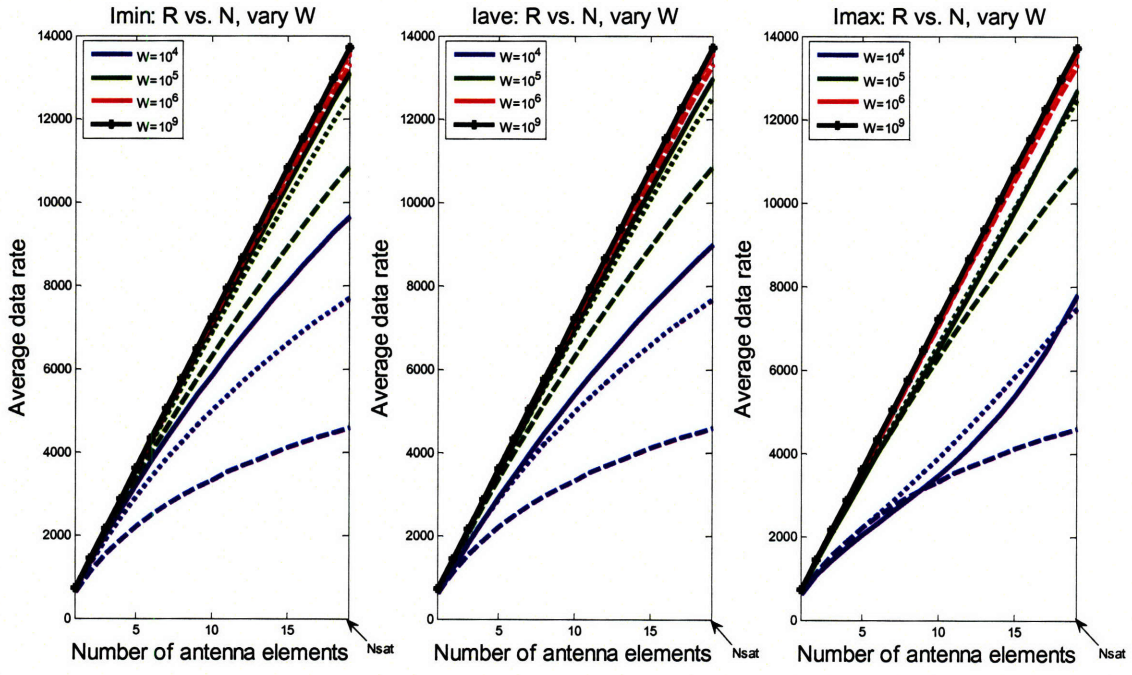

Fig. 7.6. Data rates (A, solid; B, dashed; C dotted) as a function of the number of antenna elements for minimum, average and maximum interference with increasing bandwidth, $\frac{P_{tot}}{4\pi d^2} = 1\left[\mathrm{W}/\mathrm{m}^2\right]$, ($N_{sat}$=19).

The final cases that we consider are those with nonzero interference and moderate noise power in relation to the interference. Fig. 7.7 plots the pairwise data rates as a function of N for average interference and increasing noise power density. From this plot,

we can see that there exist cases in which each of the three scheduling schemes yield the highest achievable data rates. In particular, we see that, for a given noise power and interference level, the scheduling scheme that yields the highest data rate can change as a function of the number of antenna elements, as is evident in the cross-over points between the curves in Fig. 7.7. Based on this observation, we find that, for moderate noise power in relation to interference, it is necessary to factor into consideration the number of antenna elements when determining a scheduling scheme that will yield the highest achievable data rates.

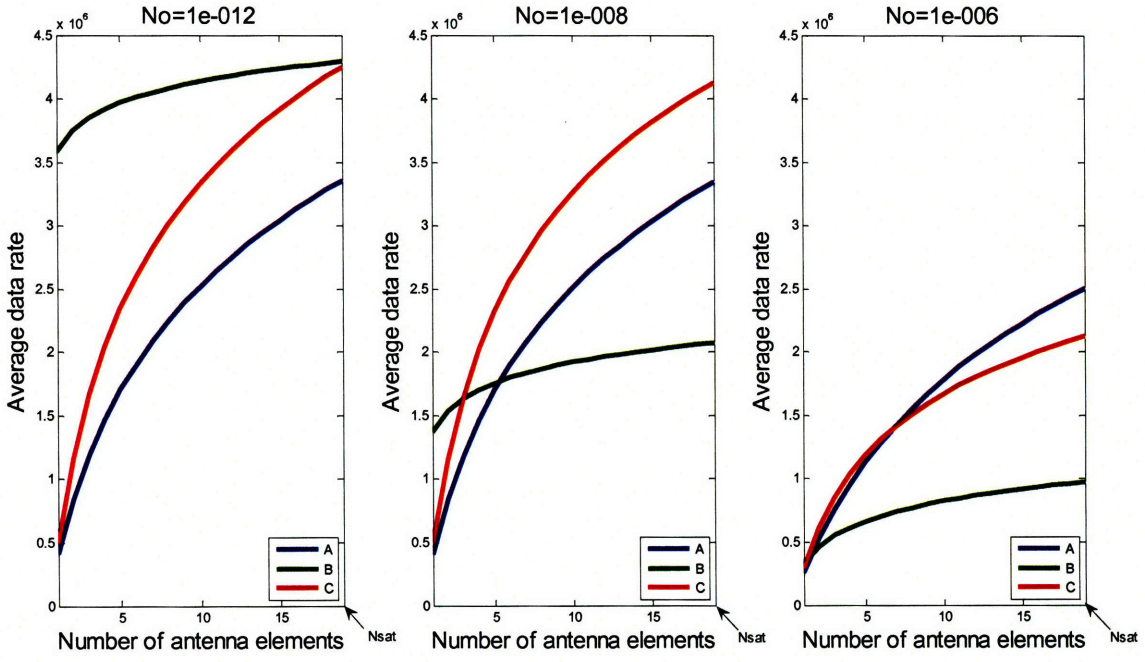

Fig. 7.7. Data rates as a function of the number of antenna elements for average interference and varying noise power density, $\frac{P_{tot}}{4\pi d^2} = 1\left[\mathrm{W}/\mathrm{m}^2\right]$, ($N_{sat}$=19).

Fig. 7.8 plots the rate curves in Fig. 7.7 with maximum interference. Comparing the achievable data rates in Fig. 7.7 and Fig. 7.8, we note the significant differences

between the achievable rates for average and maximum interference. From these plots, we find that the achievable data rates for nonzero interference and relatively moderate noise are highly sensitive to the interference modeling.

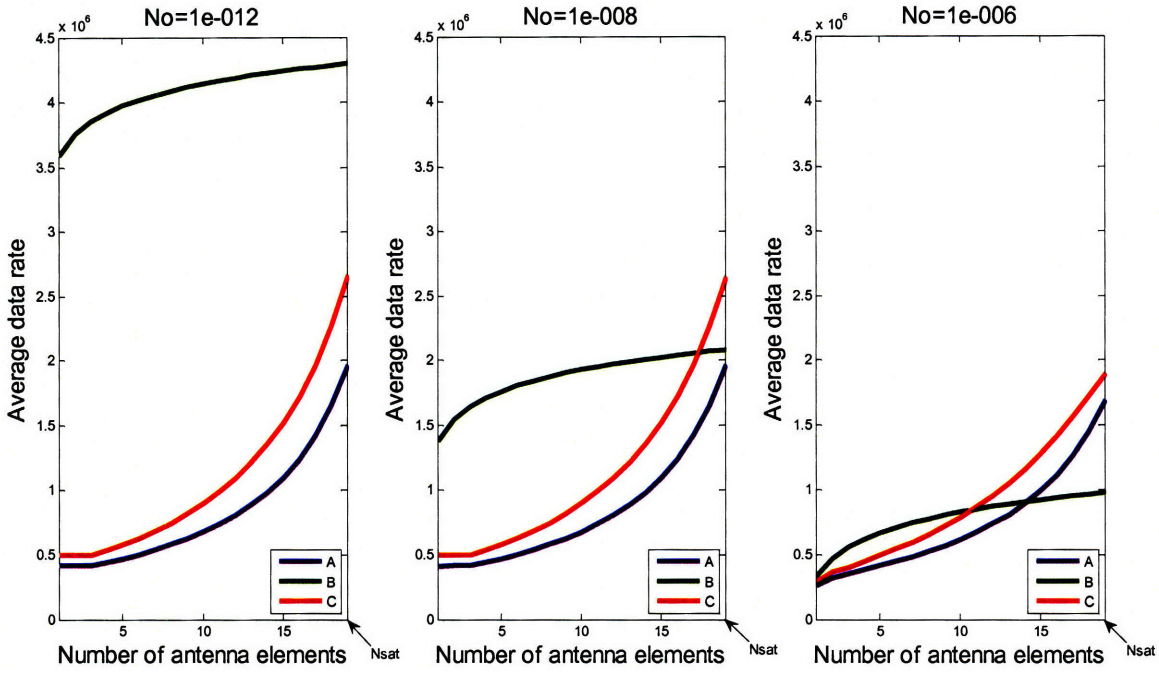

Fig. 7.8. Data rates as a function of the number of antenna elements for average interference and varying noise power density, $\frac{P_{tot}}{4\pi d^2} = 1\left[\mathrm{W}/\mathrm{m}^2\right]$, ($N_{sat}$=19).

The following table summarizes the results outlined in this chapter, comparing the achievable data rates in our simple equilateral triangle network for different scheduling schemes.

Table 7-3. Summary of comparison between data rates under Schemes *A*, *B*, and *C*.

	Scheme yielding the highest data rate
$I = 0$	*A*
$I \neq 0$ **Low Noise Power** **(severely interference-dominated)**	*B*
$I \neq 0$ **Moderate Noise Power**	Function of interference model and *N*.
Large *W* Limit **(Large Noise Power)**	*A*, *B*, *C* identical

Chapter 8

Conclusions and Future Work

Our work in this thesis studies how antenna beamforming affects achievable data rates in infrastructureless wireless networks. First, based on our model of antenna elements as isotropically radiating point sources that do not interfere with each other in any way, we derived the antenna beampattern for a uniform circular antenna array (UCAA) utilizing conventional beamforming under a maximum average power constraint. In the absence of a closed form solution for the UCAA beampattern, we made approximations to the directivity and sidelobe levels as a function of the number of antenna elements. We found that the antenna beampattern does not change significantly with increasing the number of antenna elements past a point of saturation, N_{sat}, determined by the antenna size and carrier wavelength; specifically, when the elements are spaced approximately $\frac{\lambda}{2}$ apart. Thus, the achievable data rates do not increase with increasing the number of antenna elements past N_{sat}. On the other hand, for $N<N_{sat}$, we found that the achievable data rates increase with N for all levels of interference and noise power. While we examined the antenna beampattern under our idealized antenna model, we recognize that, in reality, mutual coupling among the antenna elements can reduce directivity and distort the beampattern.

With our approximation to the receive power and interference based on analysis of the UCAA beampattern, we examined the achievable data rates in a three-user network with a symmetric network topology and uniform traffic pattern. We studied the limiting

cases under three different scheduling schemes. For very large channel bandwidth, the three scheduling schemes achieve the same data rates and the performance is noise limited. For moderate bandwidth and zero interference, the scheme in which users transmit on all links at all times yields the highest data rates. For nonzero interference and low noise power, scheduling users to take turns transmitting at orthogonal time slots offers considerable benefit over the other schemes. For nonzero interference and relatively moderate noise power, the scheduling scheme yielding the largest data rates depends on the interference levels and varies with the number of antenna elements. From our analysis of the achievable data rates in our simple three-user network, we found that, in some cases, scheduling user transmissions in orthogonal time slots can increase user data rates, but the particular scheduling scheme that maximizes the user data rates can depend on the interference model and the number of antenna elements.

In order to reduce interference in a network, future work can examine nulling, or imposing nulls in the antenna beampattern in directions of interfering users. At the heart of this work is the trade-off between maximizing directivity and minimizing interference. As indicated in [1], even with nulling, different scheduling schemes should be explored, particularly if users are not assumed to have non-overlapping mainbeams.

Additionally, while our analysis focused on gaining insight into how beamforming affects data rates in a simple network, for practical applications, future work should include examination of more general network topologies. More detailed analysis of the interference and achievable data rates can be carried out for these topologies using the expressions in Chapters 4 and 5. Approximations to the achievable data rates can be found for regular networks, otherwise, analysis will lie in simulations.

Finally, while we assume a fixed uniform traffic pattern and symmetrical network topology, future work can include an algorithmic study of adaptive beamforming and scheduling under changing traffic and network topology. Based on our observations in this thesis, the antenna modeling and parameters will play a significant role in determining the achievable data rates in these future analyses.

References

[1] J. P. Choi and V. W. S. Chan, "Joint Phased Array Antenna Gain Patterning and Scheduling for SATCOM Transmission," *IEEE MILCOMM*, 2005.

[2] H. Zhu and K.J.R. Liu, "Adaptive SINR Threshold Allocation for Joint Power Control and Beamforming Over Wireless Networks", *Proc. IEEE Vehicular Technology Conference (VTC)*, III, 1548 - 1552, Atlantic City, Oct 2001.

[3] M. Schubert and H. Boche, "Solution of the Multi-user Downlink Beamforming Problem with Individual SINR Constraints," *IEEE Trans. Veh. Technol.*, 53(1):18-28, January 2004.

[4] B. Suard, G. Xu, H. Liu and T. Kailath, "Uplink Channel Capacity of Space-Division-Multiple-Access Schemes," *IEEE Transactions on Information Theory*, 1468-1476, 1998.

[5] V. Kalinichev, "Analysis of beam-steering and directive characteristics of adaptive antenna arrays for mobile communication," *IEEE Antennas and Propagation Magazine*, vol.43, no.3, pp.145-152, 2001.

[6] C. Suarez, M. Ferrando-Bataller, and A. Valero-Noqueira, "Pattern Synthesis of Uniform Circular Arrays with Directive Elements," *IEEE Antennas and Propagation Society International Symposium*, 2812-2815, June 2004.

[7] G. M. Royer, ''Directive Gain and Impedance of a Ring Array of. Antennas,'' *IEEE Trans. Antennas Propagat.*, Vol. AP-14, pp. 566 573, Sept. 1966.

[8] I. Koutsopoulos and L. Tassiulas, "Adaptive channel assignment in SDMA-based wireless LANs with transceiver resource limitations," *EURASIP Journal on Signal Processing, Special Issue on signal processing-assisted cross-layer designs,* vol.86, no.8, pp.1879-1895, August 2006.

[9] F. Rashind-Farrokhi, L. Tassiulas, and K.J.R. Liu, "Joint Optimal Power Control and Beamforming in Wireless Networks Using Antenna Arrays," *IEEE Trans. Communications*, Vol 46, 1313-1324, October 1998.

[10] W. Rhee and J.M. Cioffi, "On the capacity of multiuser wireless channels with multiple antennas," *IEEE Trans. Inf. Theory*, vol.49, no.10, pp.2580–2595, Oct. 2003.

[11] R. Vilzmann, C. Bettstetter, and C. Hartmann, "On the impact of beamforming on mutal interference in wireless mesh networks," in Proc.IEEE Workshop on Wireless Mesh Networks (WiMesh), (Santa Clara,USA), Sept. 2005.

[12] B. Hassibi, "Multiple-Antenna Systems and Wireless Networks," *IEEE Radio and Wireless Symposium*, 63-66, January 2006.

[13] E. Telatar, N. Chiurtu and B. Rimoldi "Dense Multiple Antenna Systems", 2001 IEEE Information Theory Workshop, Cairns, Australia, September 2001.

[14] K. Sundaresan, W. Wang and Stephan Eidenbenz, "Algorithmic aspects of communication in ad-hoc networks with smart antennas," MobiHoc 2006, 298-309.

[15] A. Singh, P. Ramanathan and B. D. Van Veen, "Spatial Reuse through Adaptive Interference Cancellation in Multi-Antenna Wireless Ad Hoc Networks", Globecom'05.

[16] T. Ohira, "Emerging adaptive antenna techniques for wirelss ad-hoc networks", IEEE International Symp. Circuits Systems, ISCAS2001, IV, pp.858-861, Sydney, 2001.

[17] P. Gupta and P. R. Kumar, "The capacity of wireless networks," *IEEE Transactions on Information Theory*, vol. 46, pp. 388-404, 2000.

[18] L. Dai and V. Chan, "Proactive Topology Reinforcement of Wireless Networks," *IEEE Wireless Communications & Networking Conference (WCNC)*, 2007.

[19] J. Goodman, *Introduction to Fourier Optics*, 3rd ed., Roberts & Company, 2005.

[20] A. Kong, *Electromagnetic Wave Theory*, Wiley, New York, 1986.

[21] H. L. Van Trees, *Detection, Estimation and Modulation Theory*, part I, III. New York: Wiley, 1968.

[22] N. Amitay, V. Galindo, and C. Pang Wu, *Theory and analysis of phased array antennas*, Wiley-Interscience, 1972.